THE UNIVERSITY OF ARIZONA
Wyant College of Optical Sciences

Mueller Characterization for Partial Polarimetry

Quinn Jarecki, Doctoral Defense 5/3/24
Advisor: Meredith Kupinski, Polarization Lab

Introduction

- Polarization scattering depends on almost everything
  - Geometry, texture, material, etc.
- With polarization measurements, we can capture information about the many dependencies
- Interpreting polarization measurements to extract desired information can be complex

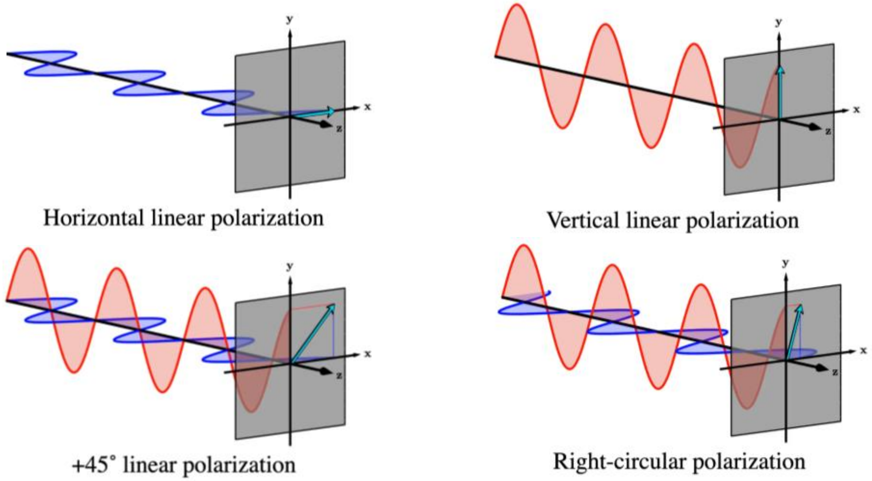

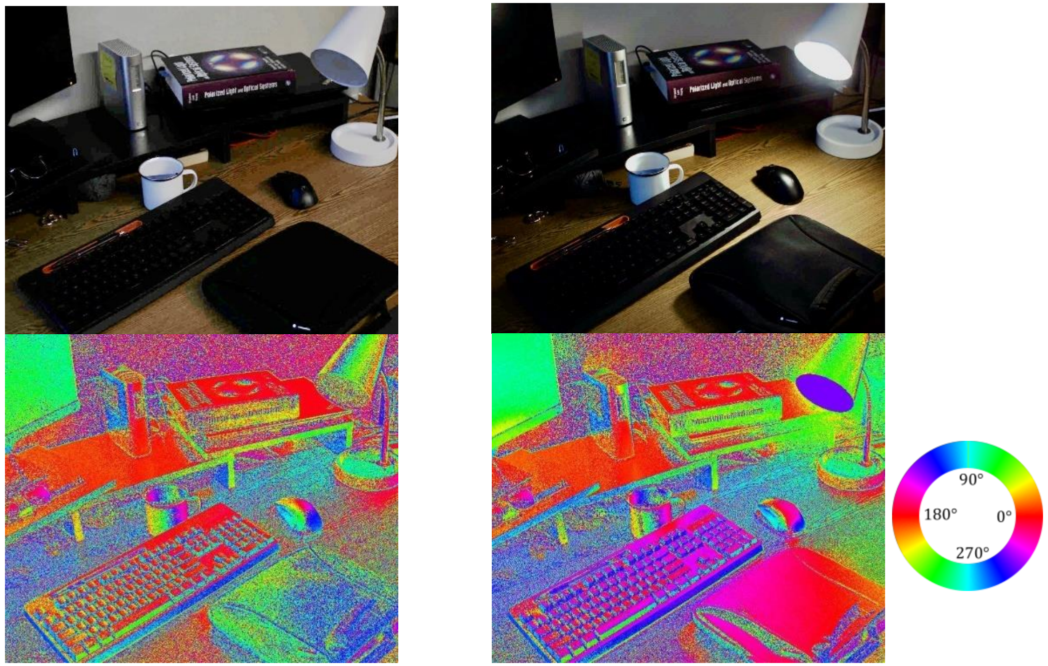

Angle of linear polarization images

https://mitsuba.readthedocs.io/en/latest/src/key_topics/polarization.html#stokes-vectors

Mueller Calculus

- Everyday environments feature polychromatic, incoherent, and/or partially polarized light is described by Stokes vectors
- Transformation of polarization by light-matter interaction is described by Mueller matrix (MM)
- MM transforms polarization via diattenuation, retardance, and/or depolarization
  - MM properties relate measurements to properties of objects such as texture, albedo, and geometry

$$\mathbf{S} = \begin{bmatrix} P_H + P_V \\ P_H - P_V \\ P_{45} - P_{135} \\ P_R - P_L \end{bmatrix} = \begin{bmatrix} S_0 \\ S_1 \\ S_2 \\ S_3 \end{bmatrix} = S_0 \begin{bmatrix} 1 \\ s_1 \\ s_2 \\ s_3 \end{bmatrix}$$

Stokes vector

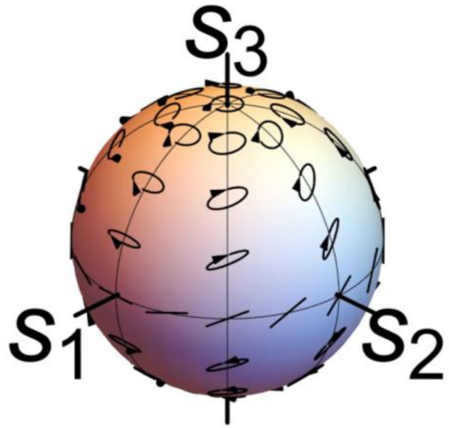

Poincaré sphere

$$\mathbf{M} = \begin{bmatrix} M_{00} & M_{01} & M_{02} & M_{03} \\ M_{10} & M_{11} & M_{12} & M_{13} \\ M_{20} & M_{21} & M_{22} & M_{23} \\ M_{30} & M_{31} & M_{32} & M_{33} \end{bmatrix} = M_{00} \begin{bmatrix} 1 & m_{01} & m_{02} & m_{03} \\ m_{10} & m_{11} & m_{12} & m_{13} \\ m_{20} & m_{21} & m_{22} & m_{23} \\ m_{30} & m_{31} & m_{32} & m_{33} \end{bmatrix}$$

Mueller matrix

Normalized Mueller matrix

Mueller Characterization

Polarimeter architecture

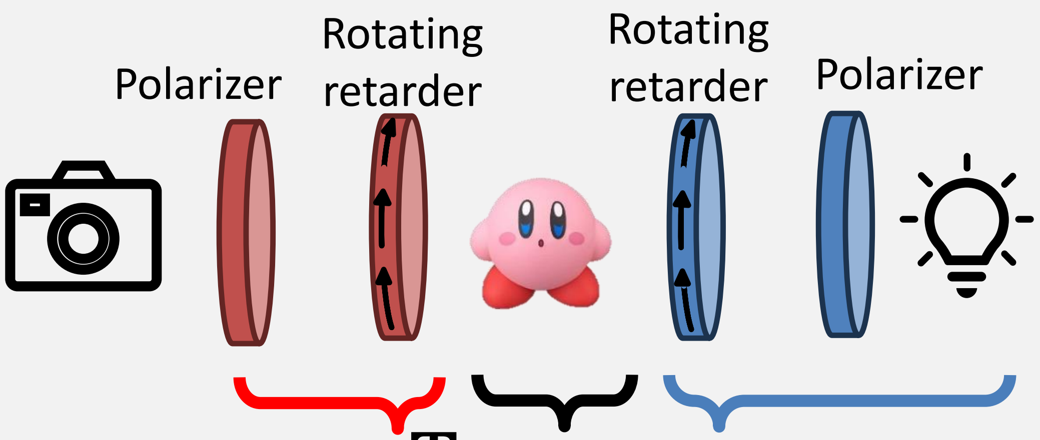

$$p = \mathbf{a}^T \mathbf{M} \mathbf{g}$$

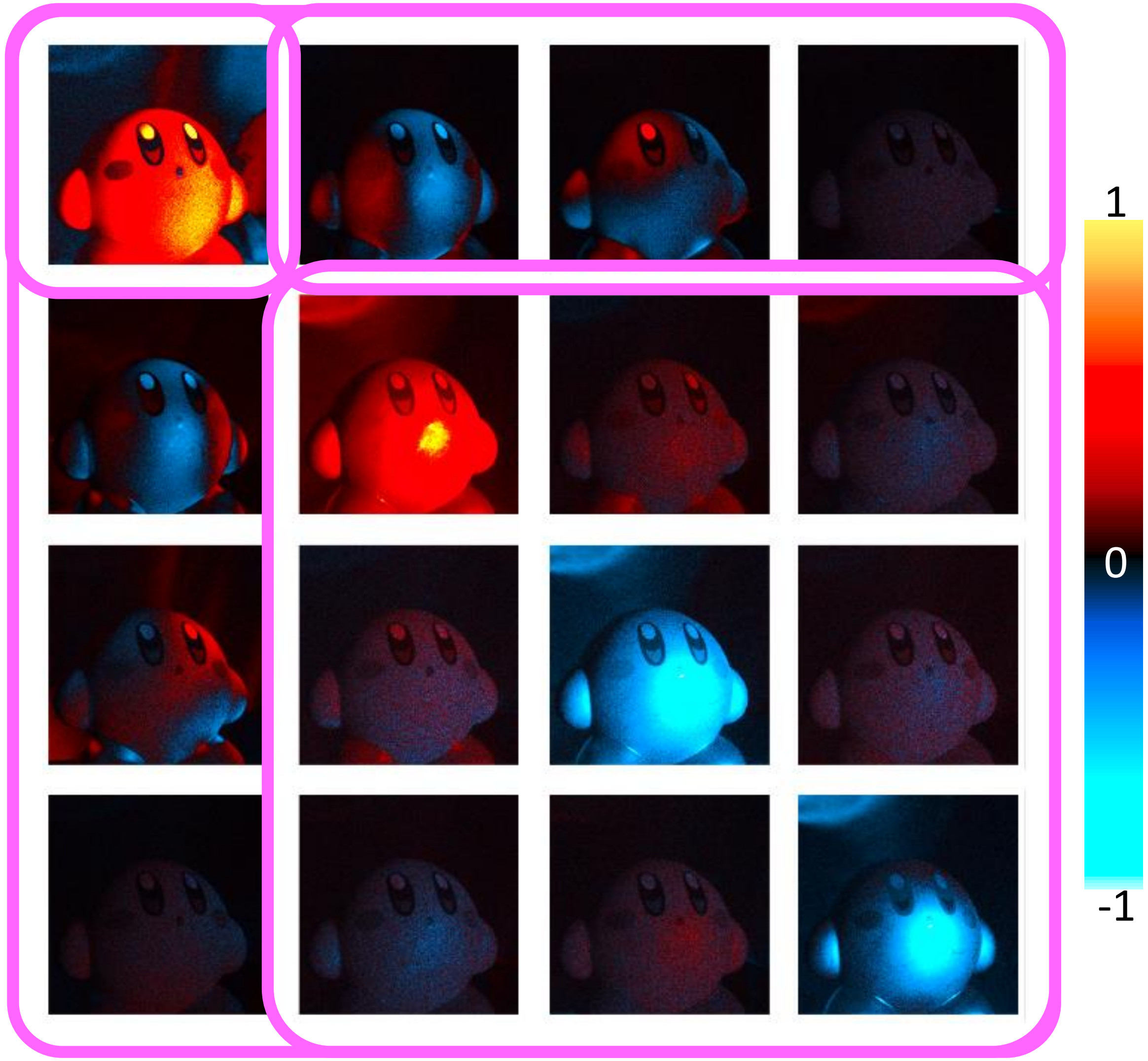

Mueller matrix image

Mueller matrix properties:

- Average reflectance: unpolarized-reflectance
- Diattenuation: polarization-dependent reflectance
- Retardance: polarization-dependent phase
- Depolarization: randomization of polarization

Simplifying Polarization Imaging

- *A priori* knowledge about polarization phenomena in an application enables simplification
  - Simplified interpretation of data
  - Simplified measurement requirements

- Contributions of this doctoral work represent different efforts to reduce some of the complexities of polarimetric imaging
  - Simplifications make insights from polarimetric information may more easily accessible in variety of applications

RGB950: Mueller polarimeter

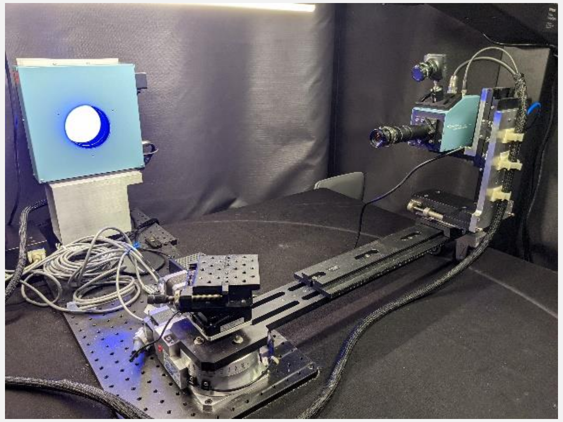

LUCID: Linear Stokes polarimeter

Complex, complete polarimetry

Simpler, partial polarimetry

Major Research Contributions

Optimizing Polariscopic Imaging for the Human Eye

- Optimization of polarization generator and analyzer states for maximizing contrast in polariscopic images of birefringent targets

Jarecki, Q., & Kupinski, M. (2024) Optimizing near-infrared polariscopic imaging for the living human eye. *Optics Express*, *32(10)*. https://doi.org/10.1364/OE.520657

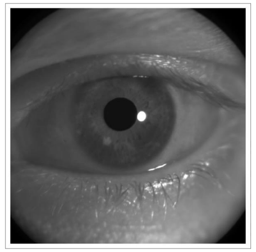

Efficient pBRDF Acquisition and Representation

- A method for efficiently acquiring and representing empirical MM data
- Requires 37% fewer goniometric measurements and stores 3 times fewer MMs per wavelength than the state-of-the-art

Jarecki, Q., & Kupinski, M. Sampling Optimization and Compact Tabulation of Isotropic Polarized Scattering. *(in preparation)*

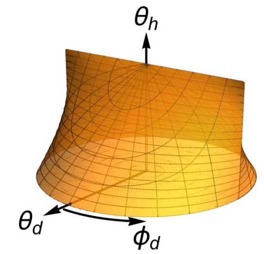

Mixed Polarization Scattering Models

- An original polarized scattering model which both decouples depolarization and mixes first-surface with diffuse polarized reflection as a function of scattering geometry,
- Average diattenuation orientation error of 10.9° and magnitude error of 8.3% when compared to measured data

Jarecki, Q., & Kupinski, M. (2024). Polarized representation for depolarization-dominant materials. *Optics Express*, *32*(5) . https://doi.org/10.1364/OE.512146

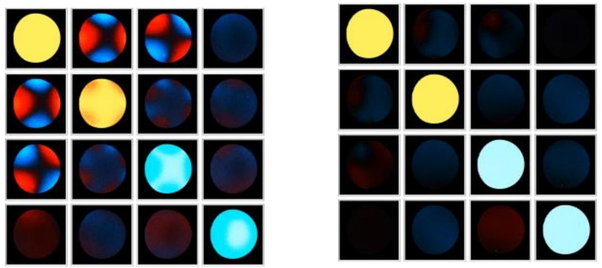

Depolarization Measurement and Mueller Extrapolation

- Partial polarimetric method for estimating depolarization magnitude and extrapolating MM
- Average error in depolarization magnitude of 7.6% and simulated polarimetric measurement error of 6.0% despite a 10× reduction in number of measurements

Jarecki, Q., & Kupinski, M. (2022). Underdetermined polarimetric measurements for Mueller extrapolations. *Optical Engineering*, 61(12). https://doi.org/10.1117/1.OE.61.12.123104

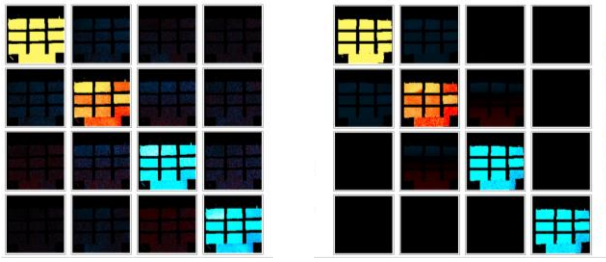

Optimizing Polariscopic Imaging for the Human Eye

Chapter 3

Partial Polarimetric Eye Measurements

Mueller image acquisition of *in vivo* human eyes

Challenges of Eye Measurements

Customize Mueller Polarimeter

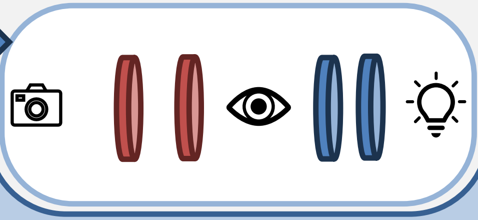

Mueller Image Data

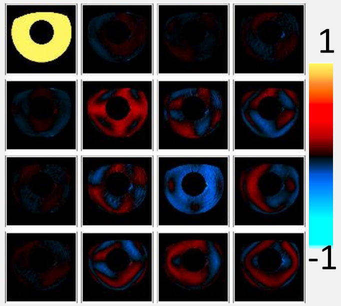

Partial polarimetry application of MM images

Analyze Mueller Image Data

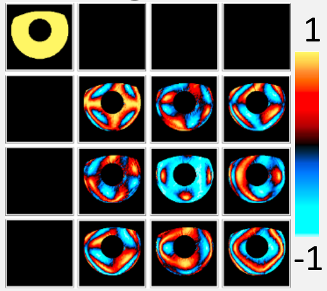

Optimize Polariscopic Configuration

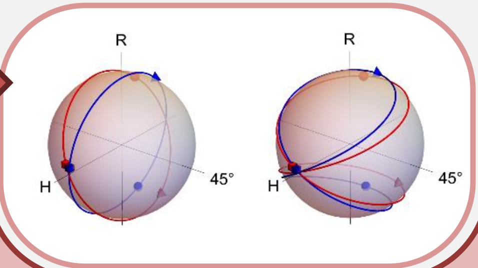

Maximized Contrast

Why the Eye?

- Corneal birefringence
  - Anisotropic collagen fibril structure in stroma
  - Spatially-varying retardance pattern
- Potential applications
  - Diagnostic tool for structural corneal diseases (dystrophies)
  - Image segmentation for eye tracking
- Challenges
  - Mueller polarimetry requires >16 images, duration on the order of 10s of seconds
  - Random, unconscious eye movements results in motion artifacts

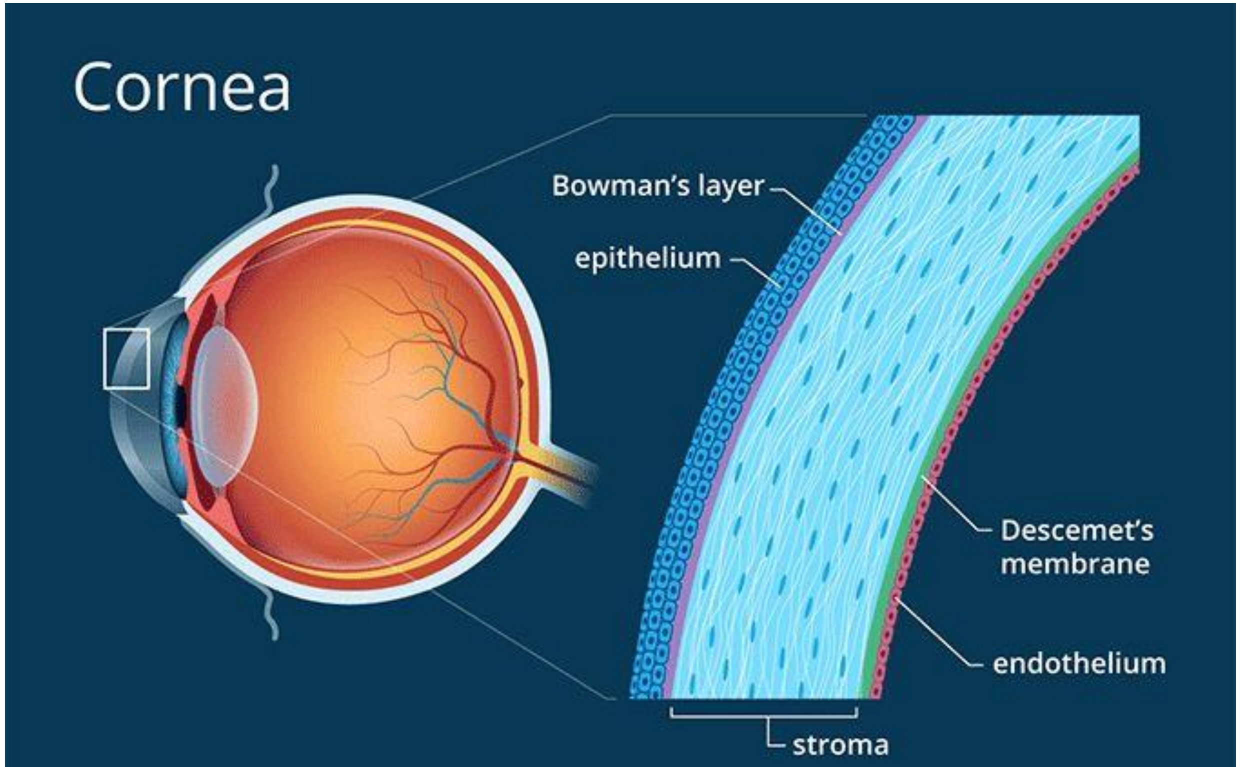

https://www.allaboutvision.com/resources/cornea.htm

Germann, James A., et al. "Quantization of Collagen Organization in the Stroma with a New Order Coefficient." *Biomedical Optics Express*, https://doi.org/10.1364/BOE.9.000173.

Stanworth, A., and E. J. Naylor. "The Polarization Optics of the Isolated Cornea." *British Journal of Ophthalmology*, https://doi.org/10.1136/bjo.34.4.201.

Modifications to Existing Polarimeter

- Modifications to full MM polarimeter for eye measurements
  - NIR wavelength operation
  - Bandpass filter + overhead lights to contract pupil
  - Reduced number of measurements (40->25)
  - Exposure time (total time of 15 seconds)
  - Image registration post processing
  - Repeated attempts for blinking

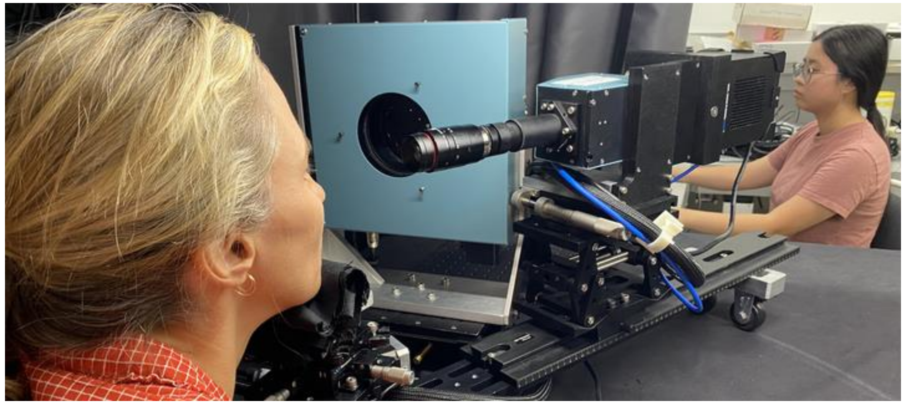

Eye measurement in RGB950

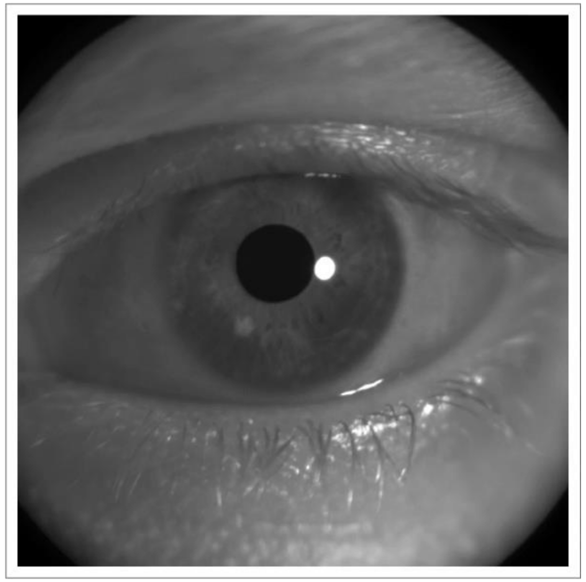

Raw image sequence

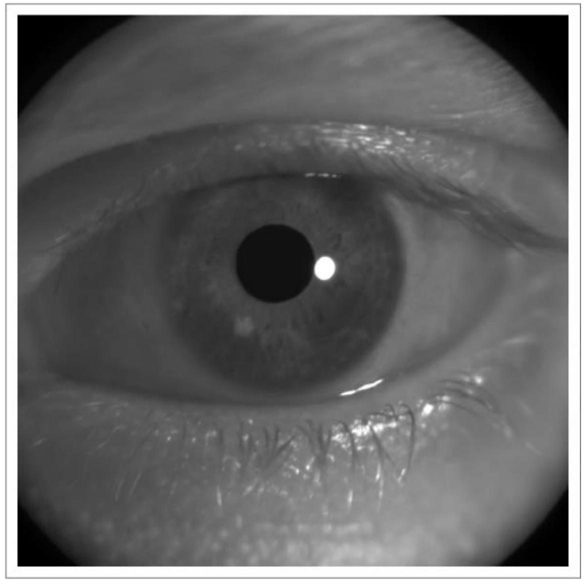

Registration applied

López-Téllez, Juan Manuel, et al. "Broadband Extended Source Imaging Mueller-Matrix Polarimeter." *Optics Letters* https://doi.org/10.1364/OL.44.001544.

Di Cecilia, Luca, et al. "Spectral Repeatability of a Hyperspectral System for Human Iris Imaging." *2018 IEEE 4th International Forum on Research and Technology for Society and Industry (RTSI)*, https://doi.org/10.1109/RTSI.2018.8548513.

MM Eye Images

- Dataset of 20 eye MM images is publicly available

- Apparent upon visual inspection:
  - Diattenuation magnitude is small
  - Depolarization is present
  - Retardance varies spatially

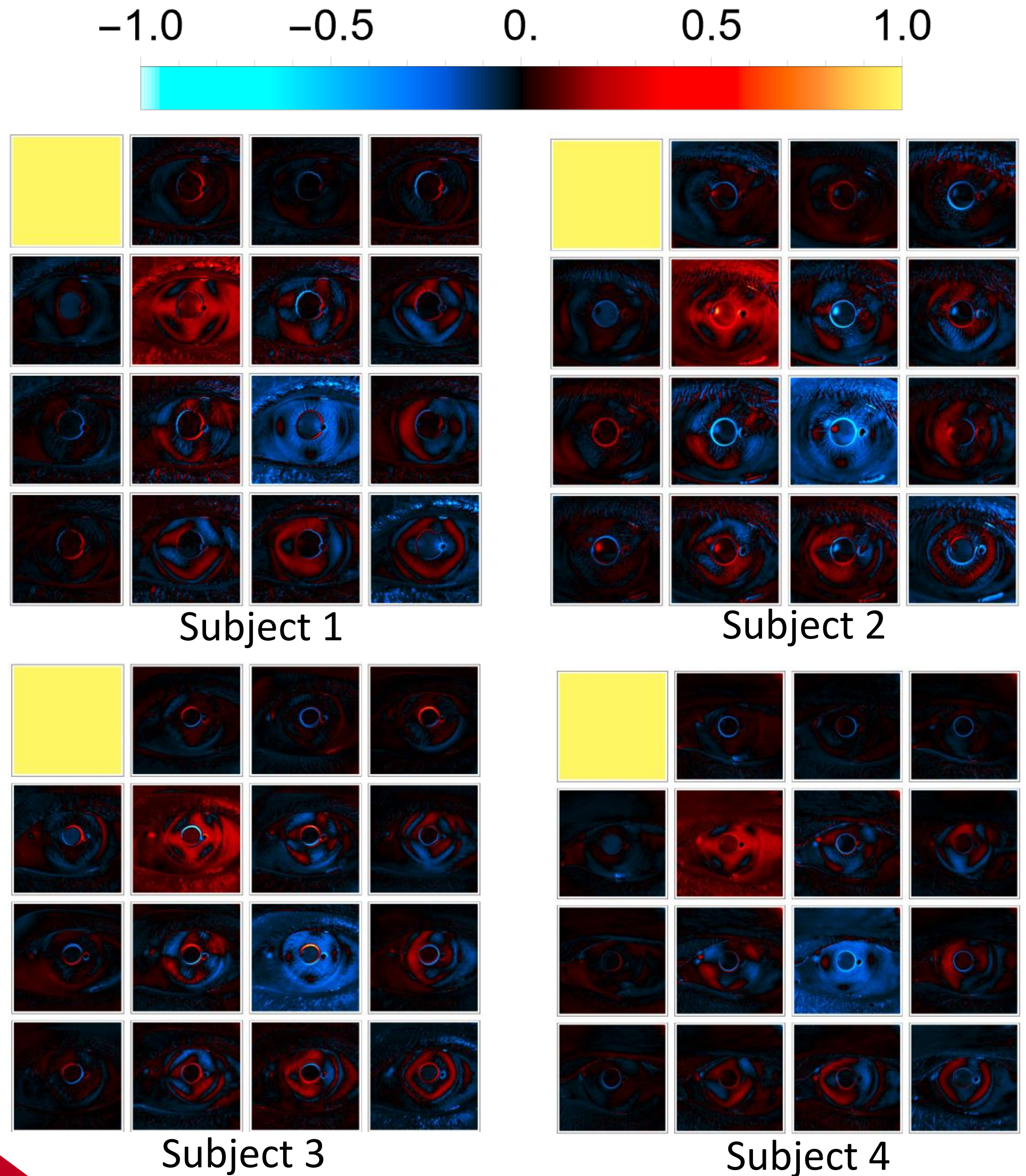

Tai, Adeline, et al. "Near-infrared human eye Mueller matrix images," https://doi.org/10.25422/azu.data.24722358

Elliptical Retardance of Cornea

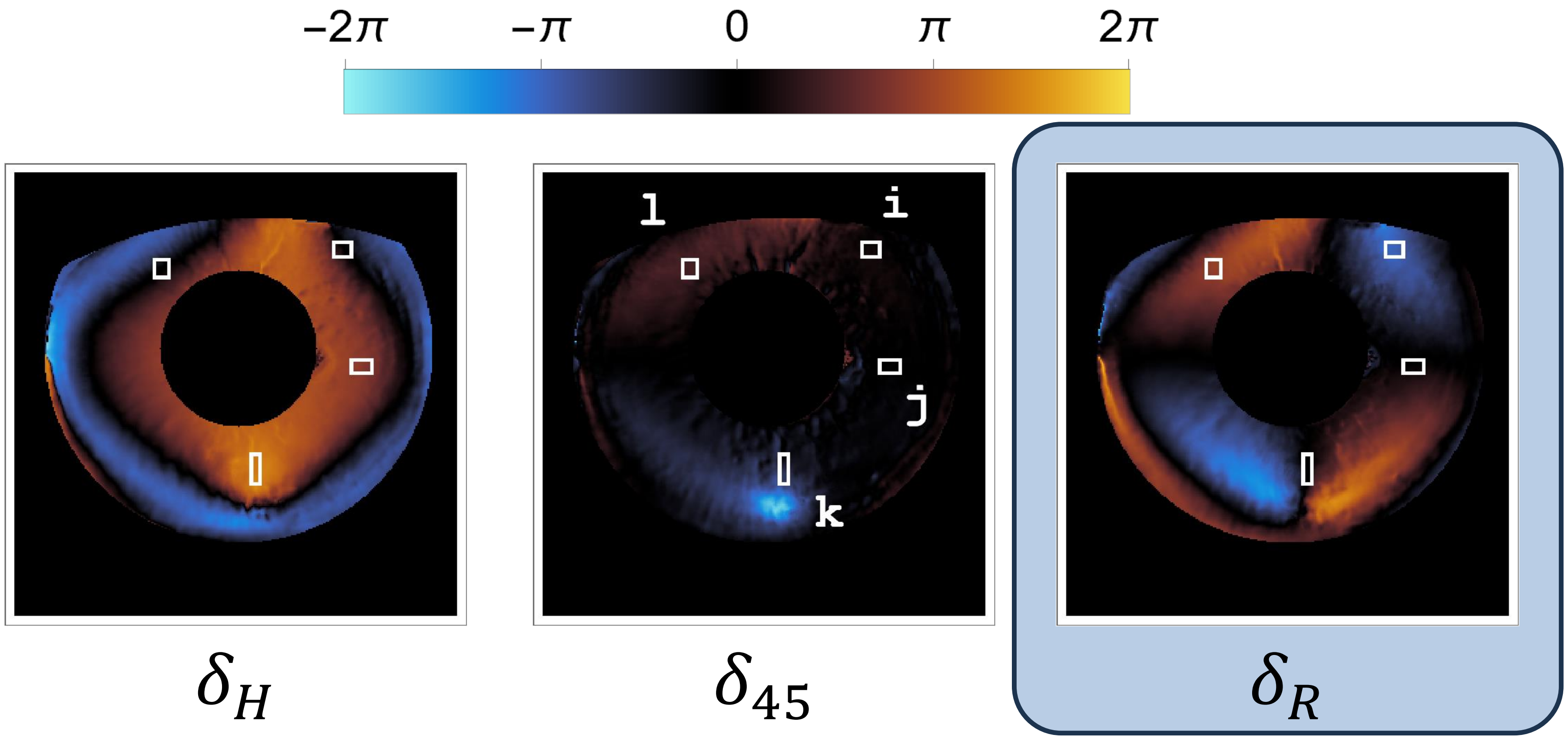

Retardance Vector Image

Jarecki, Q., & Kupinski, M. (2024) Optimizing near-infrared polariscopic imaging for the living human eye. *Optics Express*, *32(10)*. https://doi.org/10.1364/OE.520657

Partial Polarimetry Optimization with Poincaré Sphere

$$\underset{\vec{\mathbf{a}},\vec{\mathbf{g}}}{\operatorname{argmax}}\{|\vec{\mathbf{a}}\mathbf{M}_j\vec{\mathbf{g}} - \vec{\mathbf{a}}\mathbf{M}_i\vec{\mathbf{g}}|\}$$

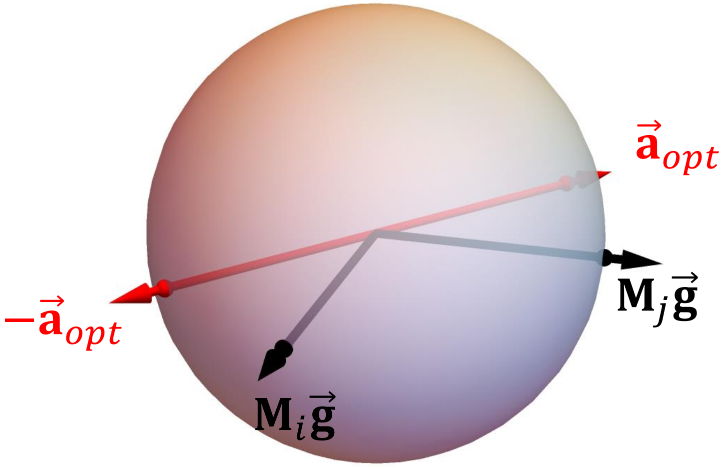

Geometric construction to find optimal analyzer

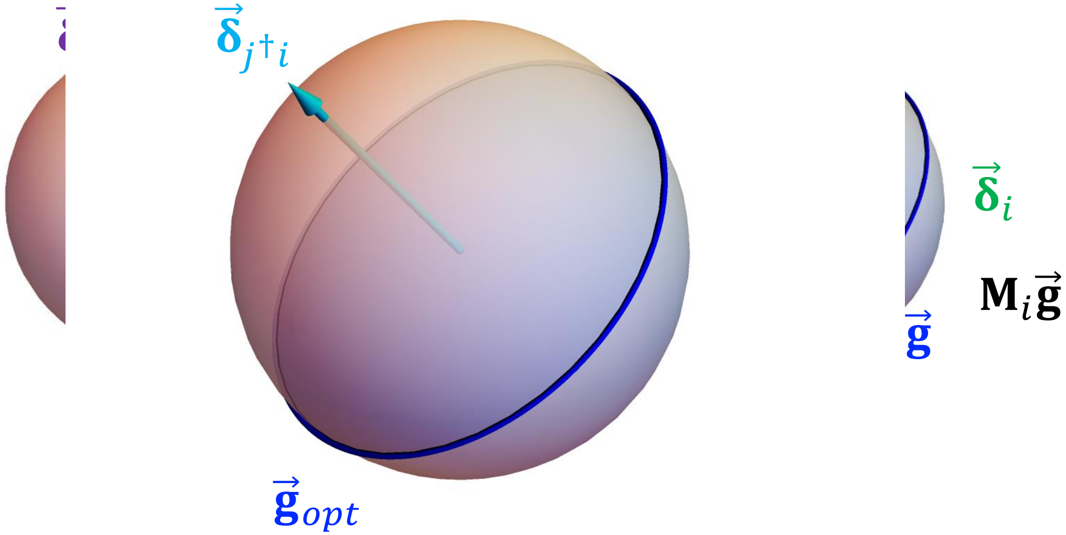

Geometric construction to find optimal generator

Optimizing Polariscopic Measurements

- There is a family of optimal solutions

- Different polariscopic pairs produce different brightness patterns
  - Expected pattern predicted based on MM

- We need to find nearly-optimal pairs available in existing hardware

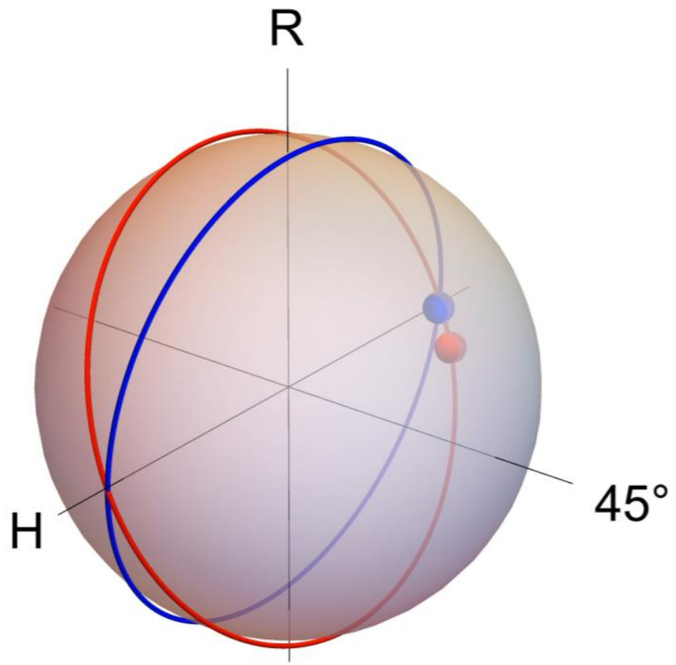

Chosen **g** and **a**

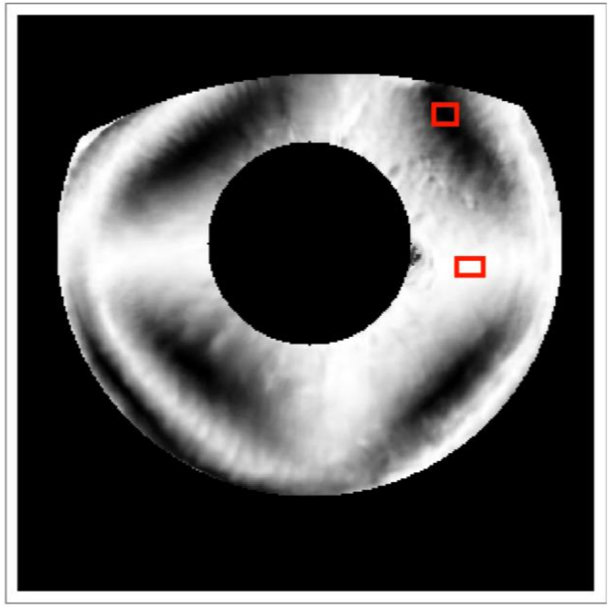

Expected Pattern in Polariscopic Image p

$$p = \mathbf{a}^{\mathrm{T}} \ \mathbf{M} \ \ \mathbf{g}$$

Choosing Available Pairs

- Need to select optimal **g** and **a** pair which has nearby available states
- Numerically determine minimum distance metric for various pairs
- Selected three pairs, expect three slightly different modulation patterns

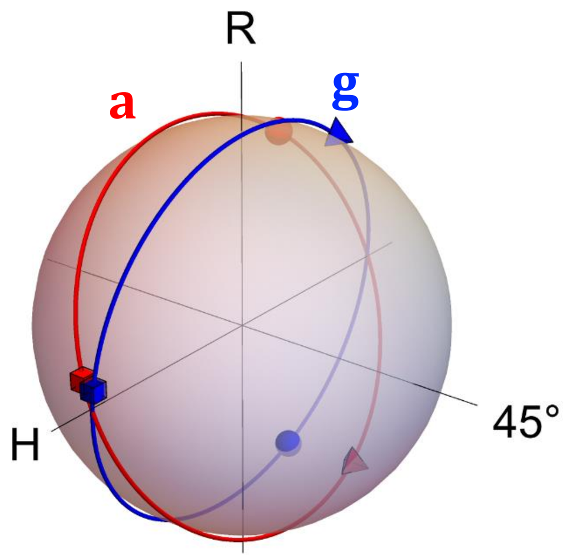

Optimal States

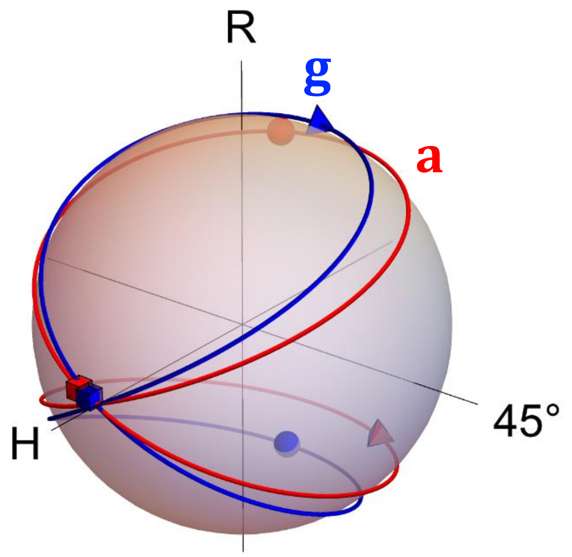

Available States

Distance from optimal

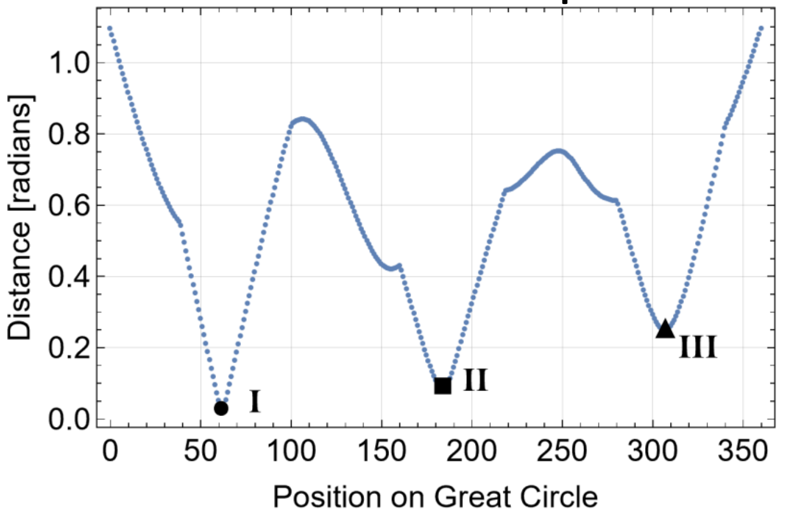

Jarecki, Q., & Kupinski, M. (2024) Optimizing near-infrared polariscopic imaging for the living human eye. *Optics Express*, *32*(10). https://doi.org/10.1364/OE.520657

Partial Polarimetric Results

- For polariscopic pairs I, II, and III, spatial pattern is predicted using original MM characterization
- Patterns show up in partial polarimetric data as expected
- Video rate captures enabled by fixed analyzer and generator

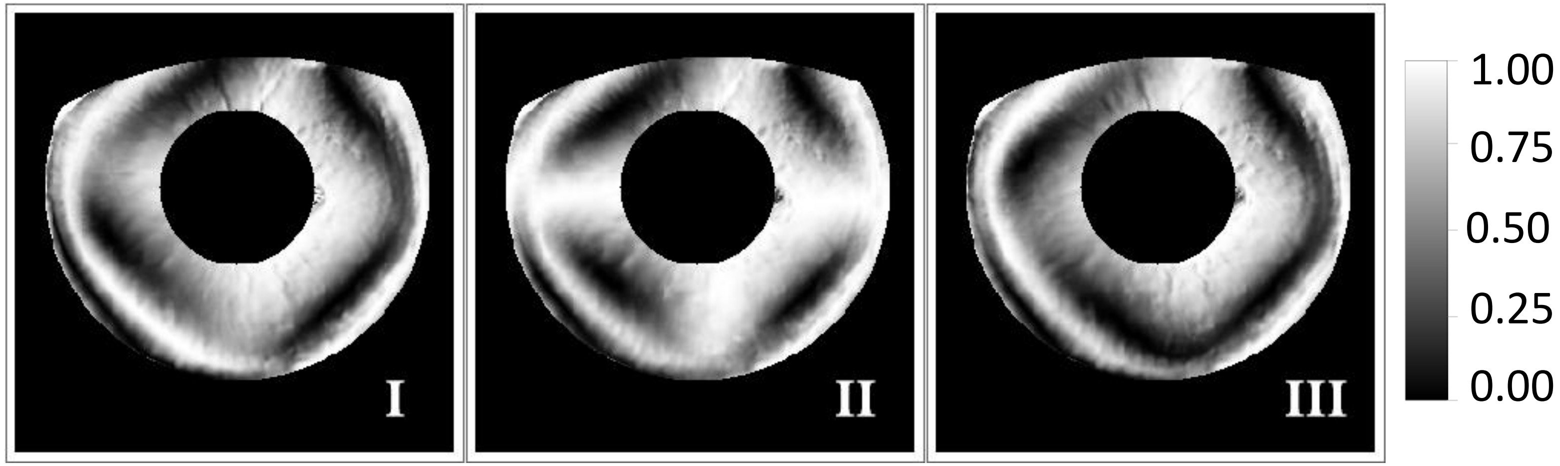

Expected patterns in polariscopic images

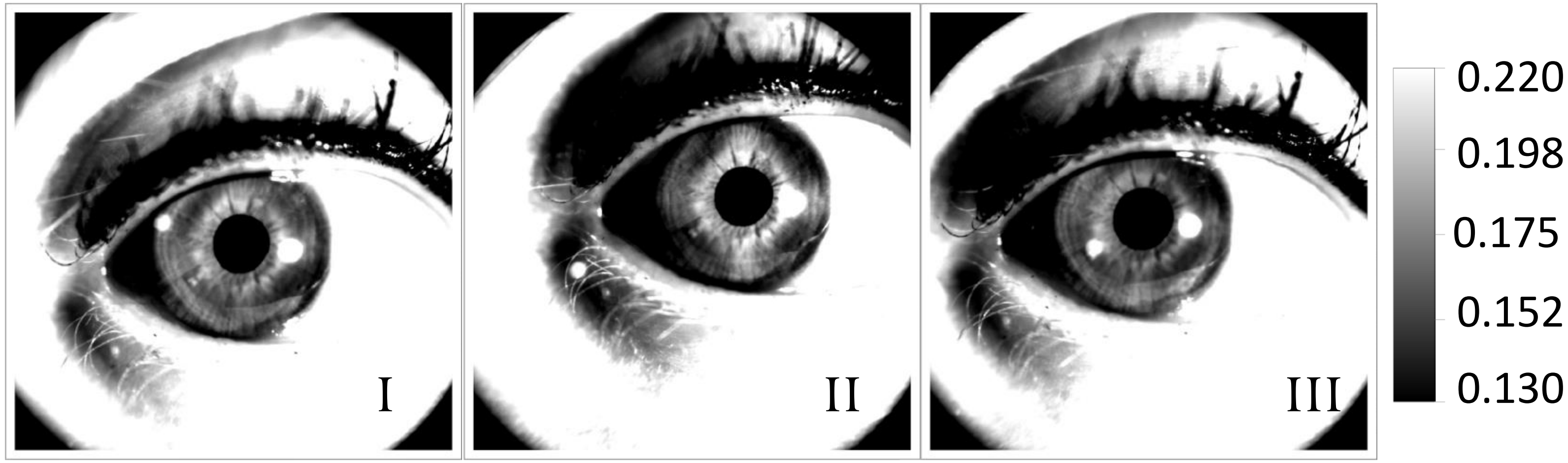

Real-time polariscopic movies!

Jarecki, Q., & Kupinski, M. (2024) Optimizing near-infrared polariscopic imaging for the living human eye. *Optics Express, 32(10)*. https://doi.org/10.1364/OE.520657

Efficient pBRDF Acquisition and Representation

Chapter 4

pBRDF Representation and Acquisition

Representation of Set of Reflection Geometries

Scattering Geometry

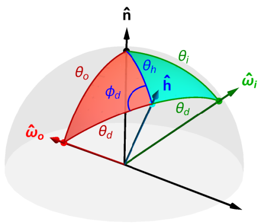

Conventional Cartesian Representation

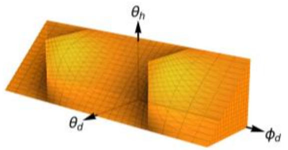

New Cylindrical Representation

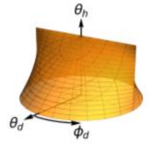

Goniometric Measurement Protocol

Analyze Sampling of Scattering Geometry

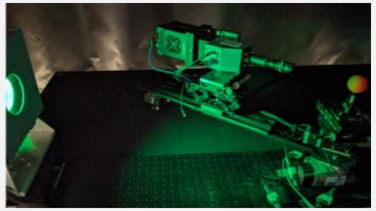

Determine Efficient Goniometer Protocol

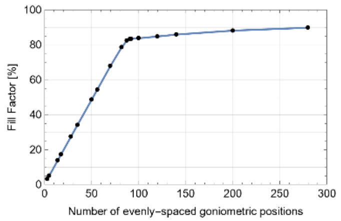

Characterize Material

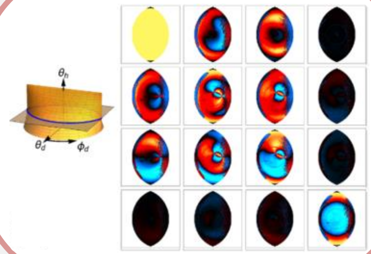

What is a pBRDF?

- Polarized bidirectional reflectance distribution function
  - MM-valued function of input and output ray geometry

- Utilized in many computer vision and physics-based rendering applications as well as remote sensing

- Empirical models are more realistic and can aid the development and validation of analytic models

Walt Disney Animation Studios. (2016, Aug 9). Disney's Practical Guide to Path Tracing. *YouTube*.

Scattering Geometry Parameterization

- Scalar and polarized BRDFs commonly parameterized with Rusinkiewicz angles
  - Better separability for analytic models
  - Reduces dimensionality for isotropic surfaces

- θ_h - determines "specularity"
- θ_d - similar to angle of incidence
- ϕ_d - determines "out-of-planeness"

- Empirical pBRDF consists of measured MM data at discrete set of $(\theta_h, \theta_d, \phi_d)$

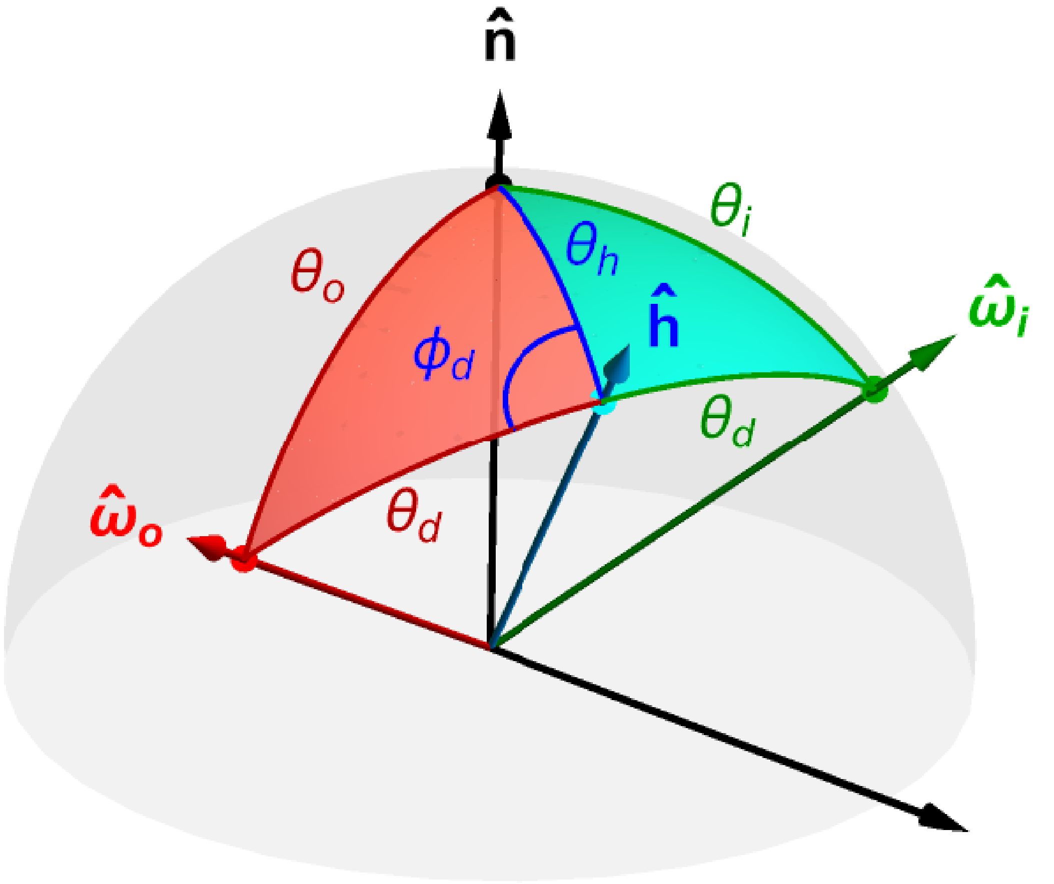

pBRDF Representation – Region of Reflection Geometries

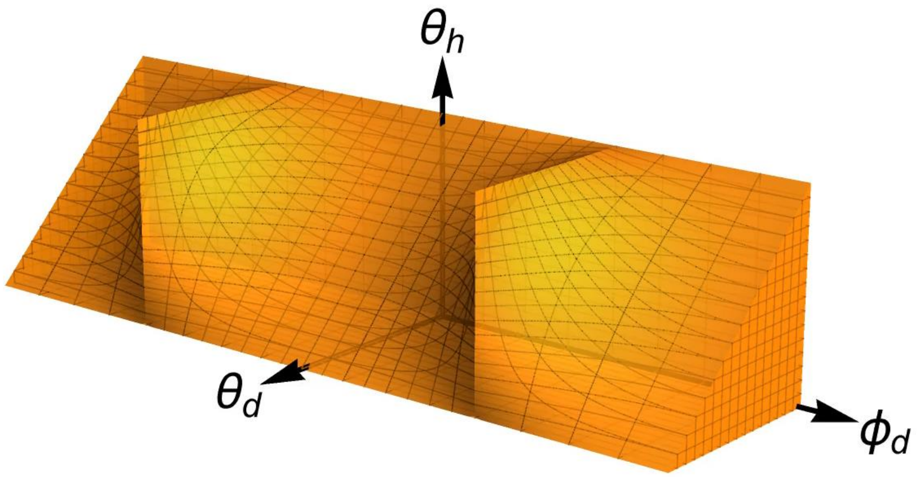

$(\theta_d, \phi_d, \theta_h)$ as (x, y, z) Cartesian coordinates

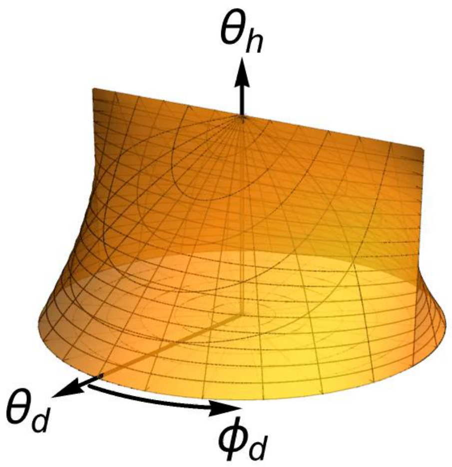

$(\theta_d, \phi_d, \theta_h)$ as (ρ, ϕ, z) cylindrical coordinates

	Cartesian	Cylindrical
Volume of reflection region	9.567	5.686
Volume of convex hull	14.217	6.633
Discrete data points	2,989,441	1,086,904

Designing pBRDF Acquisition Protocol

- pBRDF acquisition = MM measurement at many, many, many scattering geometries
- What target shape to measure?
- What set of camera angles Ω should be used to most efficiently sample scattering geometries?

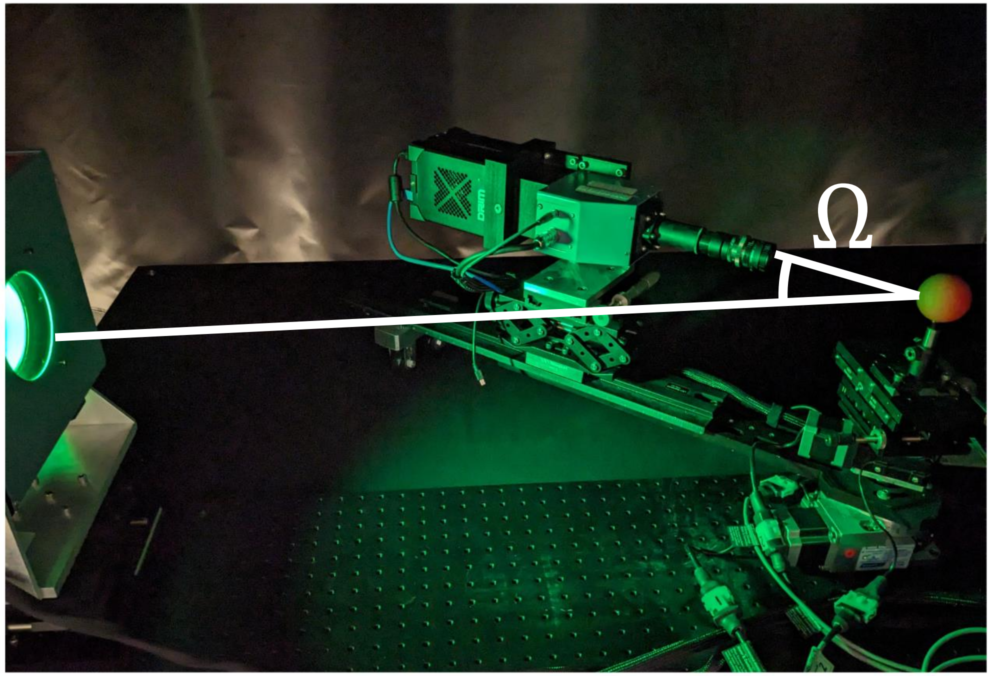

Geometries sampled using a sphere

Geometries sampled using a plane

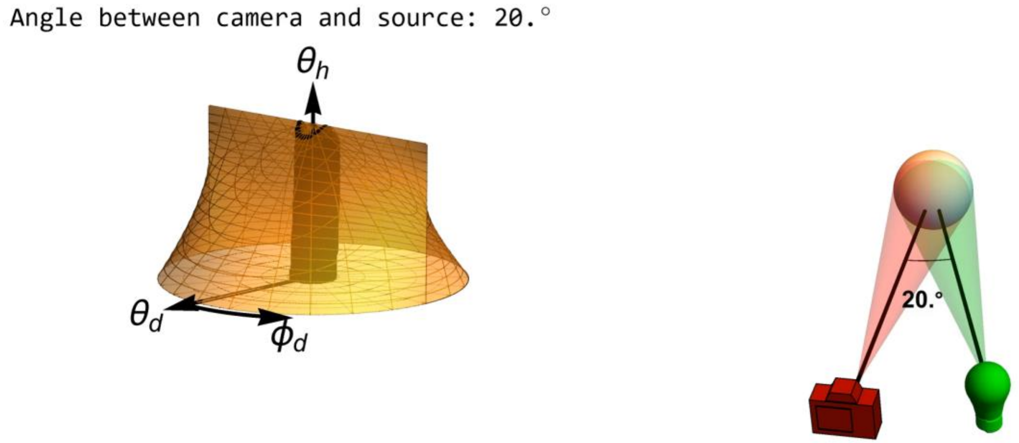

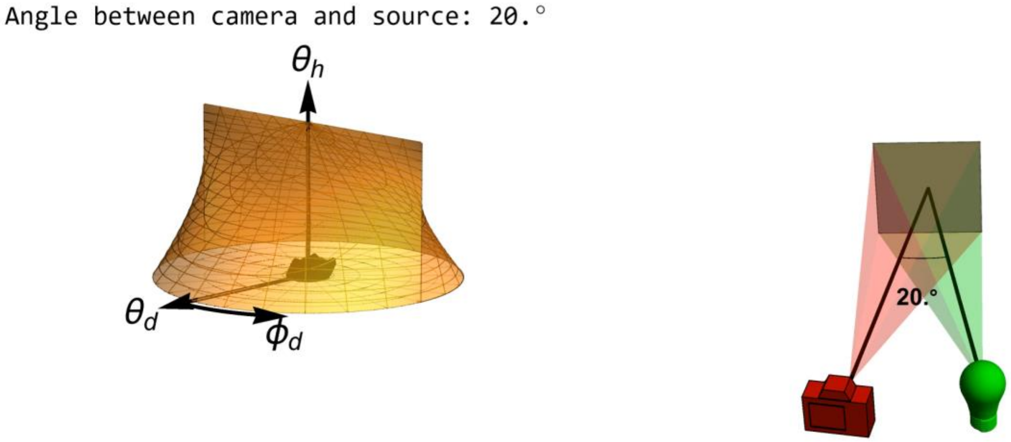

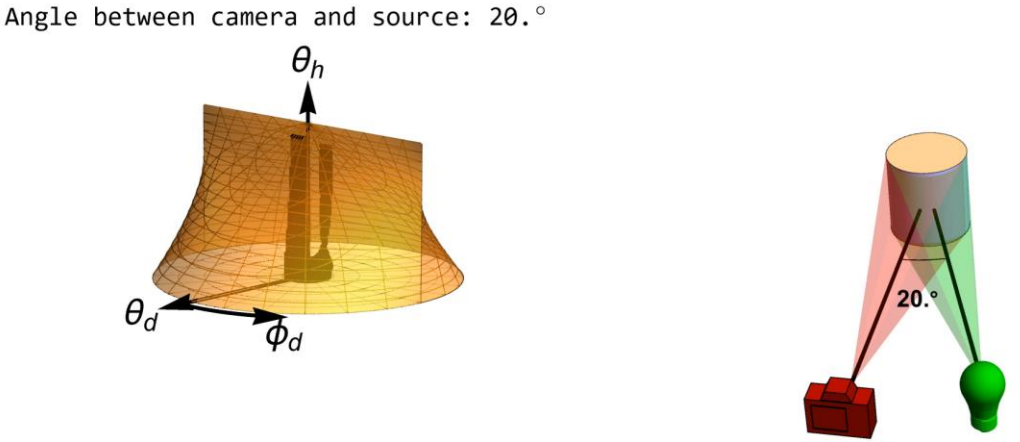

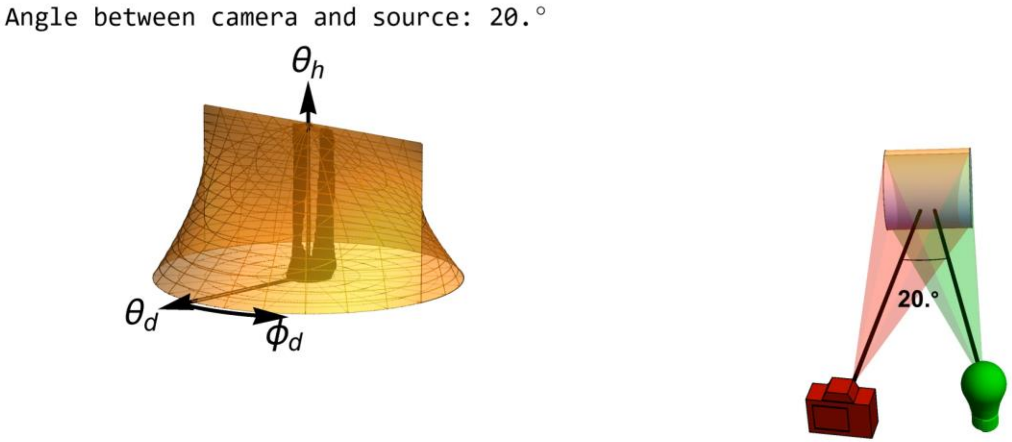

pBRDF Acquisition Protocol

- For our setup, diminishing returns at around 92 positions
  – State-of-the-art pBRDF database used 147 positions

- Corresponds to 82% of scattering geometries measured
  – 3.5% geometries inaccessible due to camera/source collision

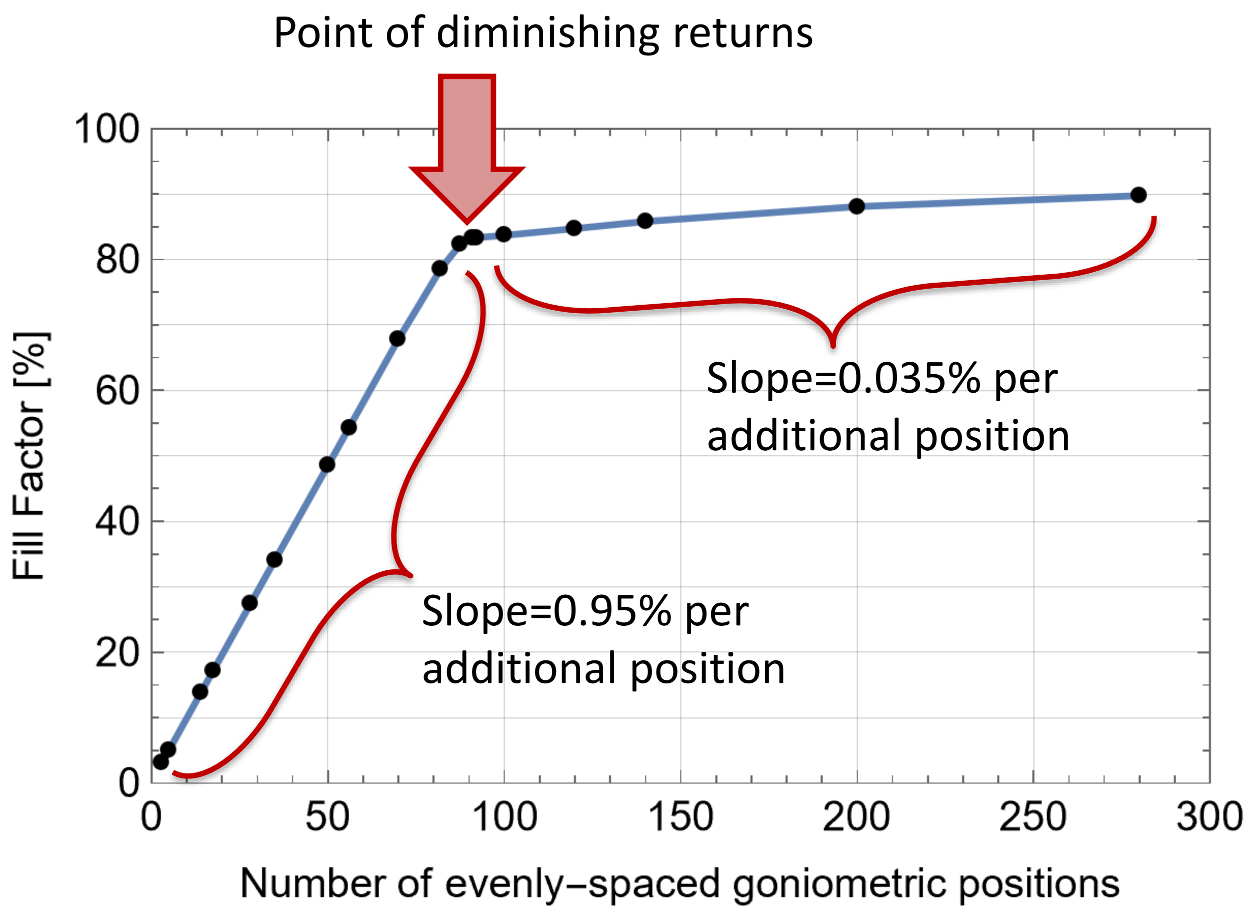

Empirical pBRDF Cross-sections

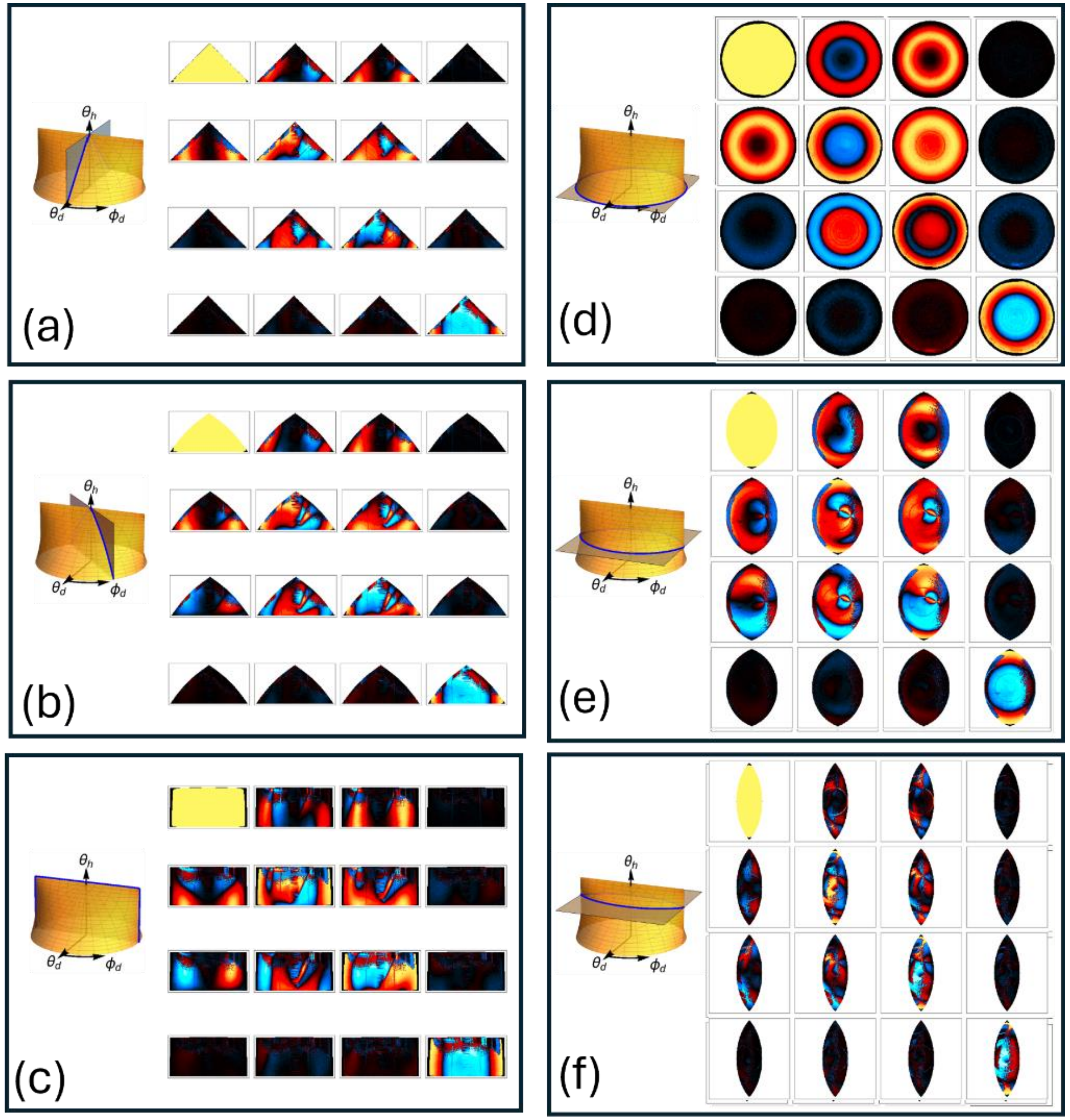

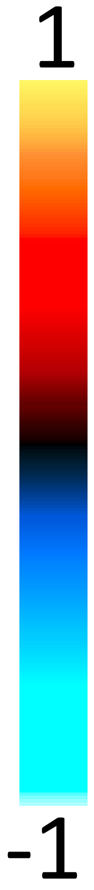

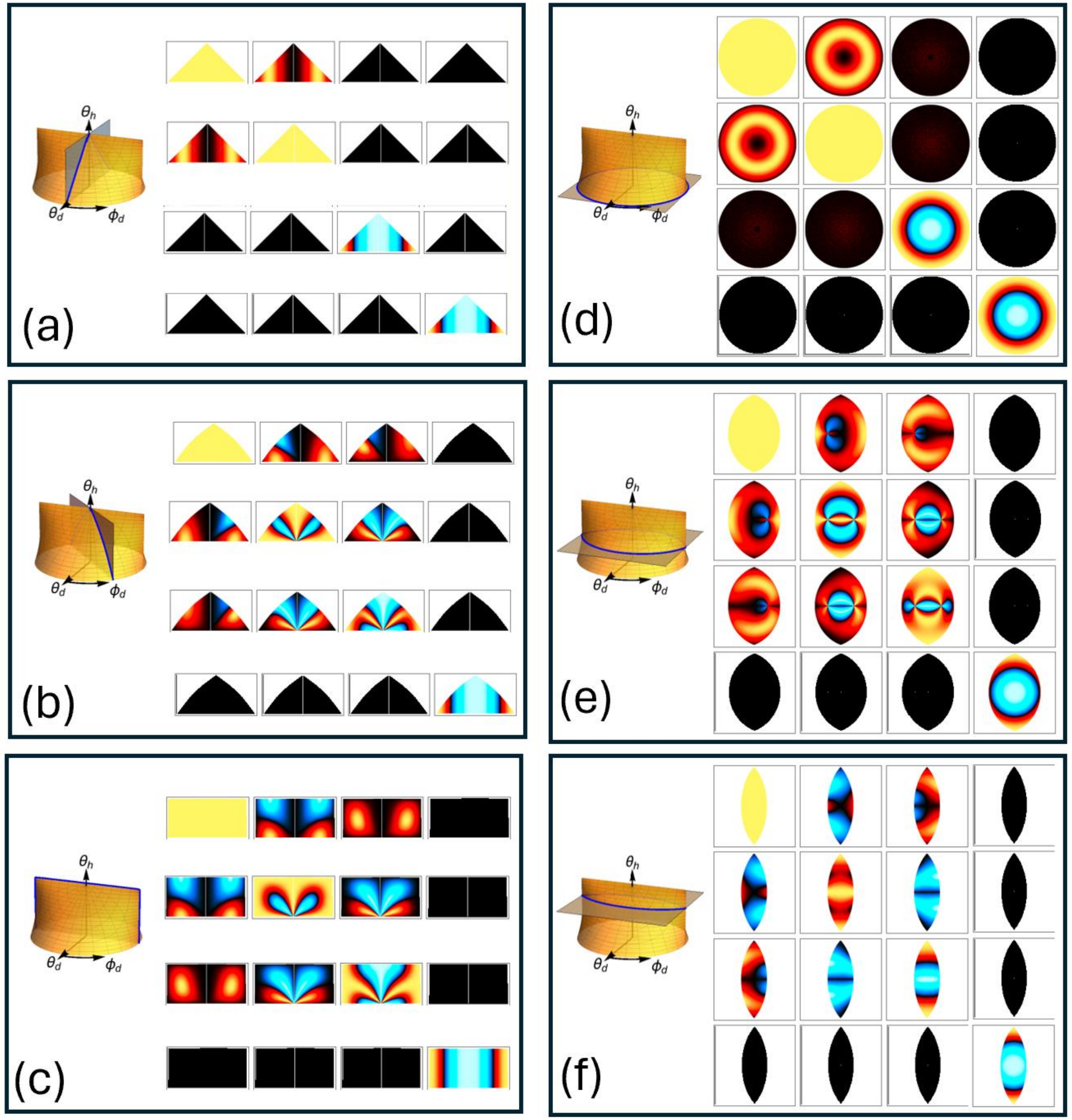

Red sphere under 451 nm (low albedo)

Fresnel reflection (simulated)

Tabulated pBRDF File Comparison

	KAIST	UA
Goniometer positions	147	92
MMs per wavelength	2,989,441	1,086,904
File size per wavelength	304 MB	110 MB
Non-reflection geometries?	Included	Excluded
Redundant geometries?	Included	Excluded
Usable directly in rendering engine?	Yes	No (not yet)

Baek, Seung-Hwan, et al. “Image-Based Acquisition and Modeling of Polarimetric Reflectance.” ACM Transactions on Graphics, vol. 39, no. 4, 12 Aug. 2020

Jarecki, Q., & Kupinski, M. “Sampling Optimization and Compact Tabulation of Isotropic Polarized Scattering.” (in preparation)

Mixed Polarization Scattering Models

Chapter 5

Mixed Polarization Scattering Models

Representation of Set of Reflection Geometries

First-surface and Diffuse Polarization

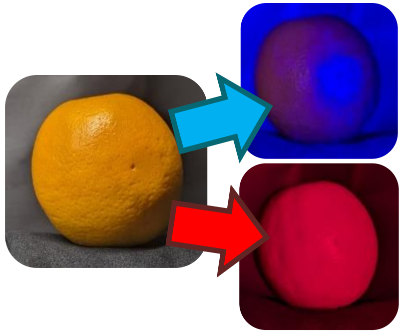

Decoupling Depolarization

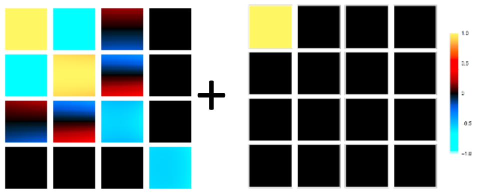

Combine Terms as a Function of Geometry

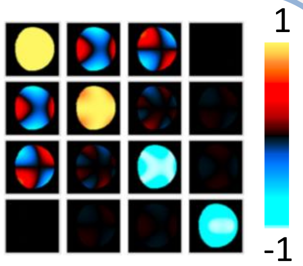

Analytic pBRDF Models

- Analytic pBRDF models are generally much more convenient for practical applications

- Analytic models frequently contain:
  - "Specular" component that describes light scattered from first surface of material
  - Diffuse component attributed to light scattered into then out of material
  - Depolarizer term

- Realistic models need to combine these as a function of scattering geometry
  - Tricky because summation of MMs can introduce depolarization in complicated ways

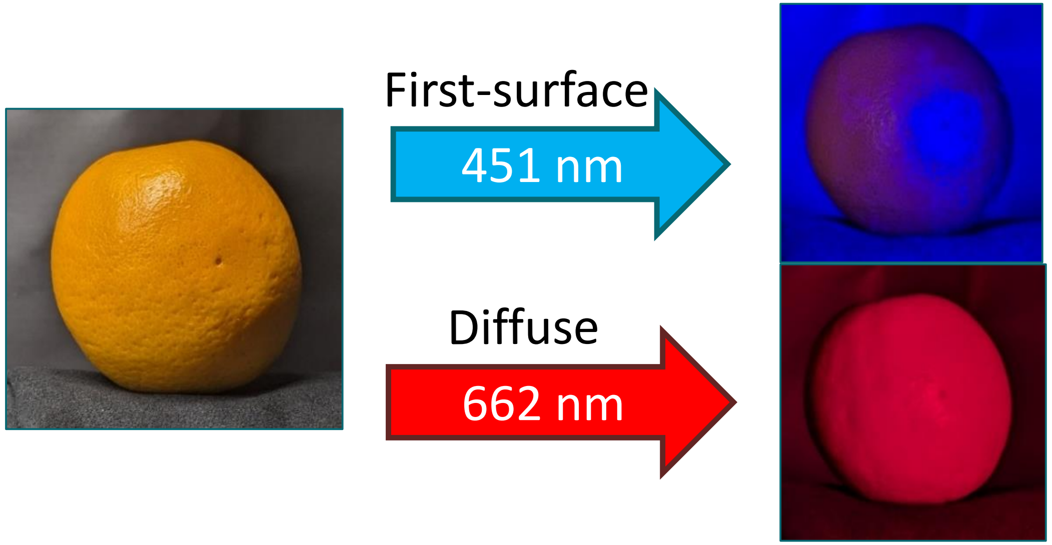

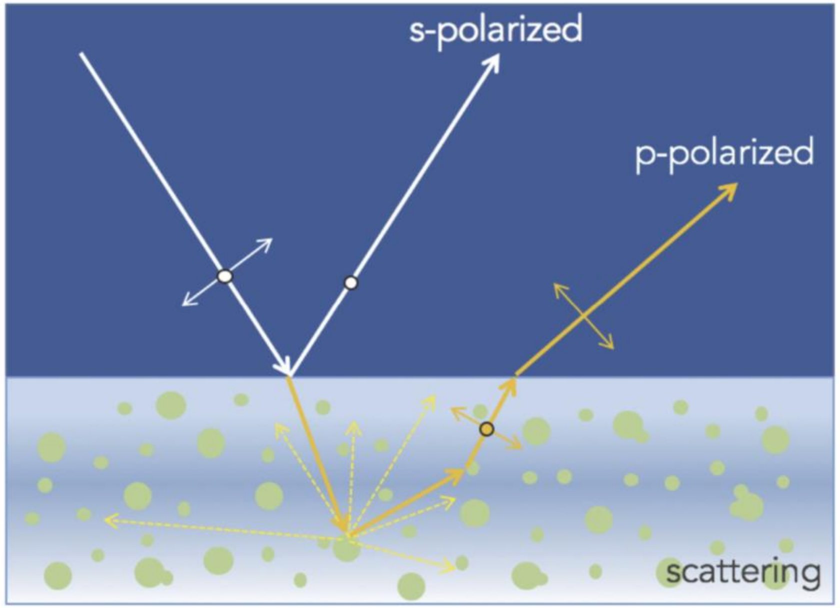

First-surface vs diffuse scattering

Kupinski, M., Bradley, C., Diner, D., Xu, F., Chipman, R., & Univ Arizona, C. O. S. (2019). Angle of linear polarization images of outdoor scenes. *58*.

Triple-degenerate MM Model

- Strongly depolarizing MMs are well-approximated by first-order depolarization model

- Degrees of freedom reduced from sixteen to eight:
  - one for throughput, M_{00}
  - one for depolarization, ξ_0
  - six for dominant non-depolarizing process $\widehat{\mathbf{M}}_0$ which describes diattenuation and retardance

Triple-degenerate MM:

$$\mathbf{M} = \frac{4M_{00}}{3}\left[\left(\xi_0 - \frac{1}{4}\right)\widehat{\mathbf{M}}_0 + (1-\xi_0)\,\mathbf{M}_{ID}\right]$$

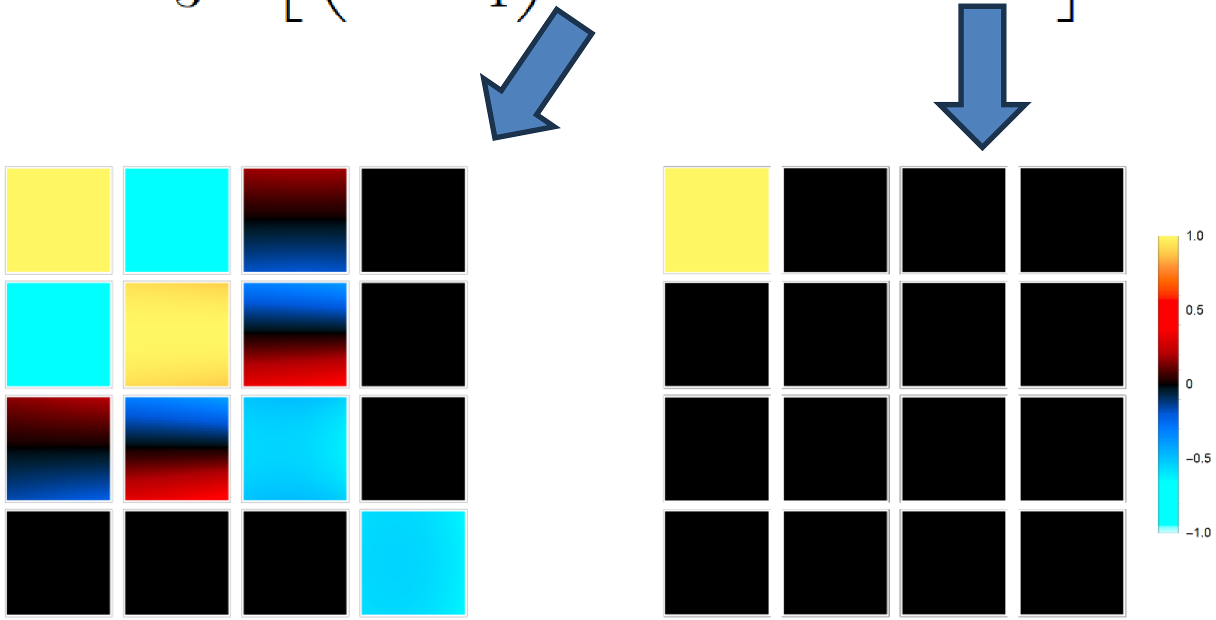

Non-depolarizing term

Ideal depolarizer

First-surface and Diffuse Polarization

- First-surface modeled as Fresnel reflection from sub-resolution microfacet
  - Diattenuation magnitude depends only on θ_d

$$\mathbf{F}_{n_\lambda}(\widehat{\boldsymbol{\omega}}_i, \widehat{\boldsymbol{\omega}}_o) = \begin{bmatrix} \widehat{\mathbf{x}}_{PSA} \\ \widehat{\mathbf{y}}_{SA} \end{bmatrix} \begin{bmatrix} \widehat{\mathbf{s}}_o \\ \widehat{\mathbf{p}}_o \end{bmatrix}^{\mathsf{T}} \begin{bmatrix} r_s(n_\lambda, \theta_d) & 0 \\ 0 & r_p(n_\lambda, \theta_d) \end{bmatrix} \begin{bmatrix} \widehat{\mathbf{s}}_i \\ \widehat{\mathbf{p}}_i \end{bmatrix} \begin{bmatrix} \widehat{\mathbf{x}}_{PSG} \\ \widehat{\mathbf{y}}_{PSG} \end{bmatrix}^{\mathsf{T}}.$$

- Diffuse modeled as polarizer with transmission axis oriented at ϕ_d

$$\mathbf{S}(\widehat{\boldsymbol{\omega}}_i, \widehat{\boldsymbol{\omega}}_o, \widehat{\mathbf{n}}) = \begin{bmatrix} 1 & 0 \\ 0 & -1 \end{bmatrix} \mathbf{R}(\phi_d) \begin{bmatrix} 1 & 0 \\ 0 & 0 \end{bmatrix} \mathbf{R}(-\phi_d),$$

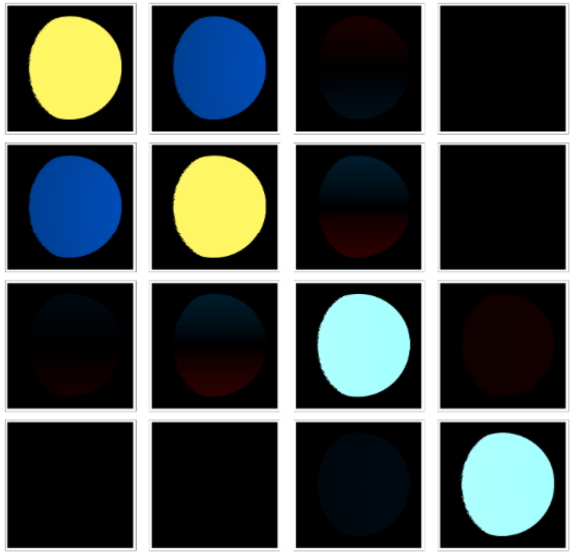

First-surface term for sphere

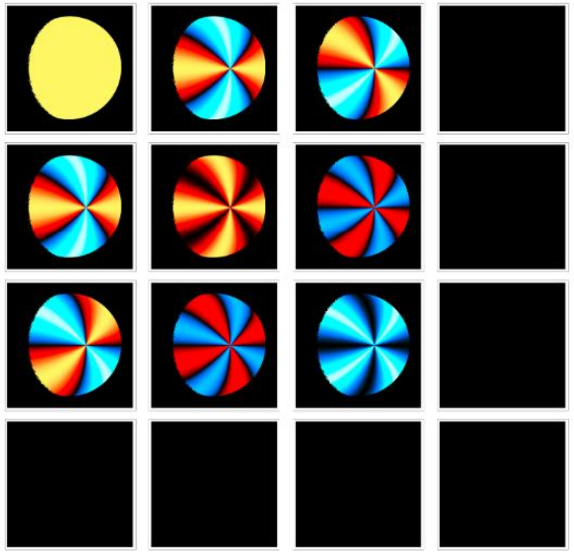

Diffuse term for sphere

Mixed Polarization Model

- Combine terms as Jones matrices
  - Keeps depolarization decoupled from dominant process

- Relative contribution to normalized MJM is a function of scattering geometry:

$$\mathbf{J}(\widehat{\boldsymbol{\omega}}_i, \widehat{\boldsymbol{\omega}}_o, \widehat{\mathbf{n}} | n_\lambda, a_\lambda, b_\lambda) = \mathbf{F}_{n_\lambda} + a_\lambda \sin^{b_\lambda}(\theta_h)\mathbf{S}(\widehat{\mathbf{n}}).$$

Material constants	451 nm	662 nm
$n_\lambda + i\kappa_\lambda$	$1.20 + 0.25i$	$1.30 + 0.08i$
a_λ	0.03	0.17
b_λ	2.5	2.0

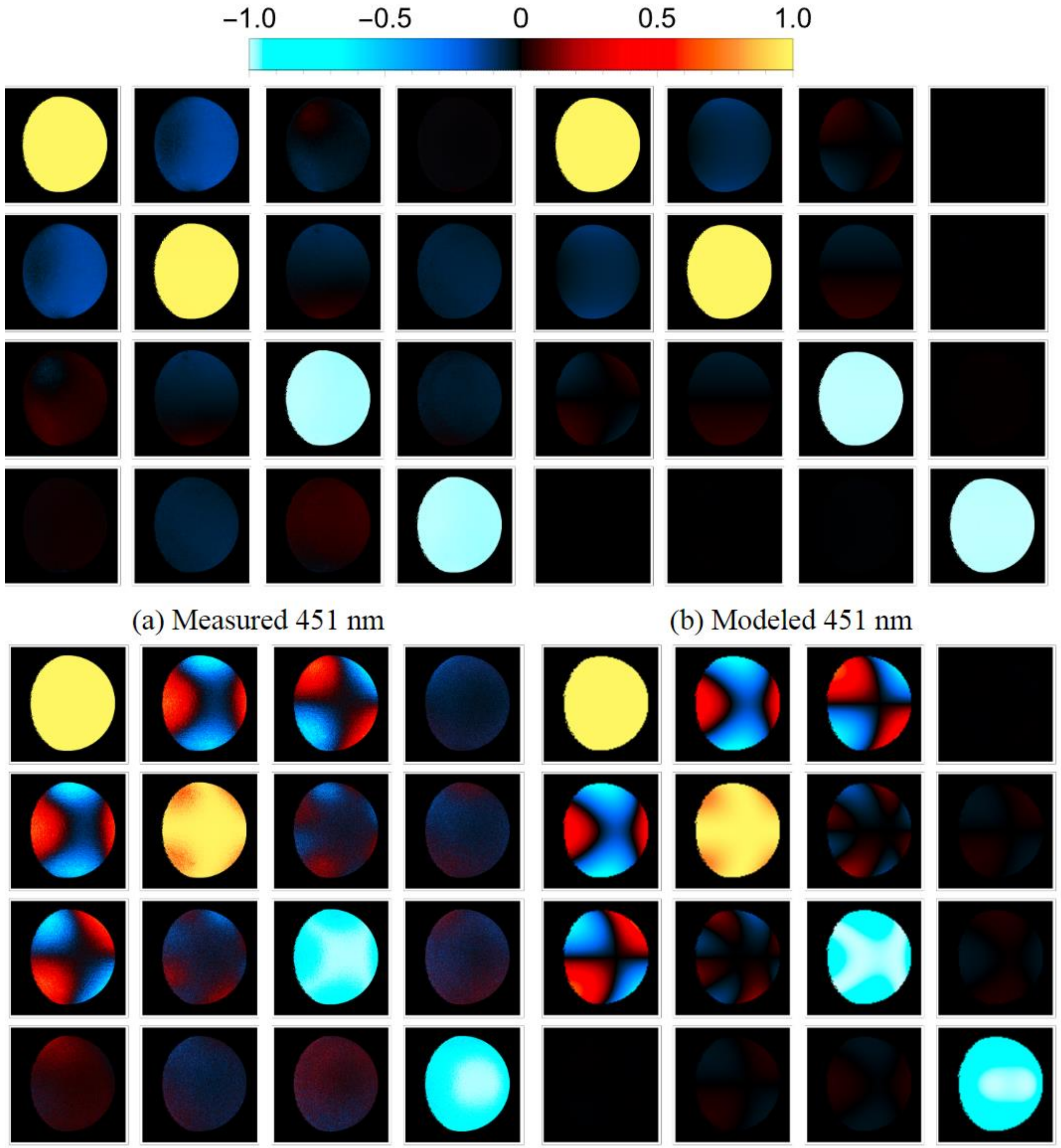

(a) Measured 451 nm (b) Modeled 451 nm
(c) Measured 662 nm (d) Modeled 662 nm

Diattenuation Comparison

- Diattenuation orientation images show match in spatial trend
- Pixel-wise errors low for 451 nm which has less spatial variation, higher errors for 662 nm

> - Over wavelength and geometry, average diattenuation orientation error of 10.9° and magnitude error of 8.3%

Diattenuation orientation images

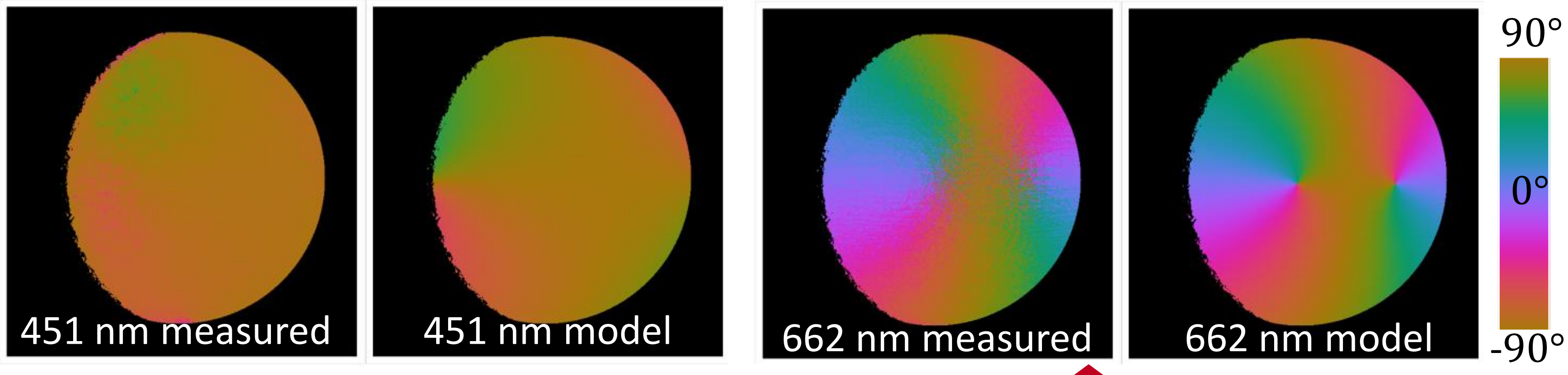

Average diattenuation magnitude

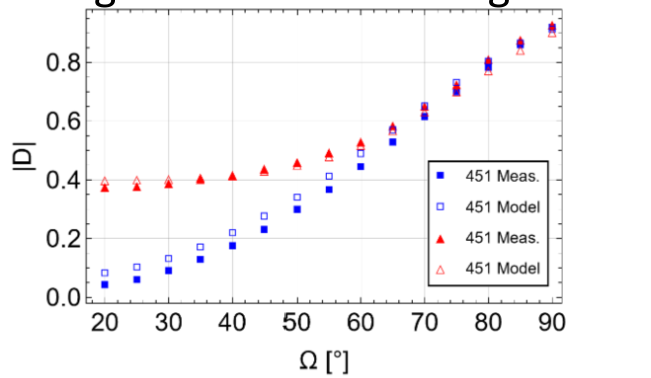

Pixelwise magnitude error

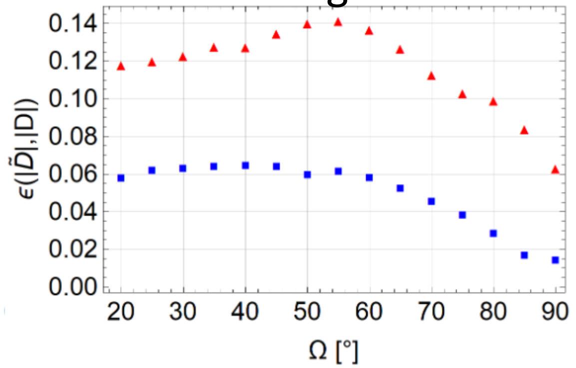

Pixelwise orientation error

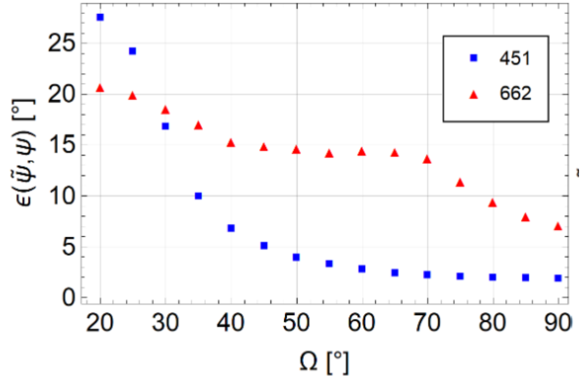

Depolarization Measurement and Mueller Extrapolation

Chapter 6

Depolarization Measurement and Mueller Extrapolation

Mueller Image Extrapolation Enabled by Models

Objects Described By
Triple-Degenerate Model

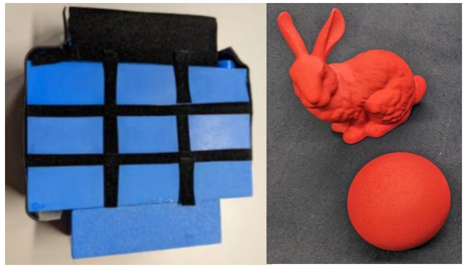

Partial Polarimetric
Measurements

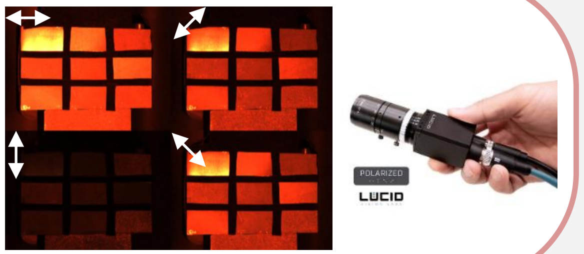

Depolarization and
Extrapolated MM

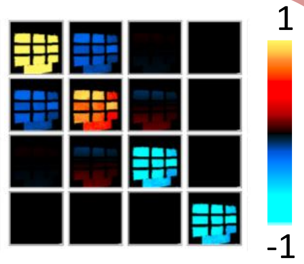

Linear Estimator for Depolarization Magnitude

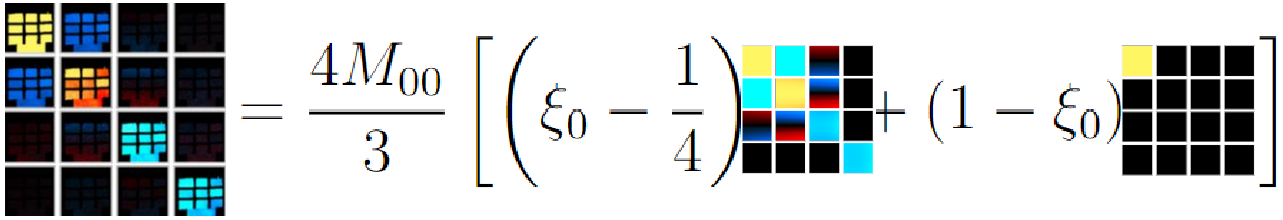

- If $\hat{\mathbf{m}}_0$ is known, TD model has two remaining degrees of freedom

- pBRDF model from previous section enables estimation of depolarization magnitude from as few as two measurements

- With ξ_0 estimate, simply plug back into TD model to extrapolate MM

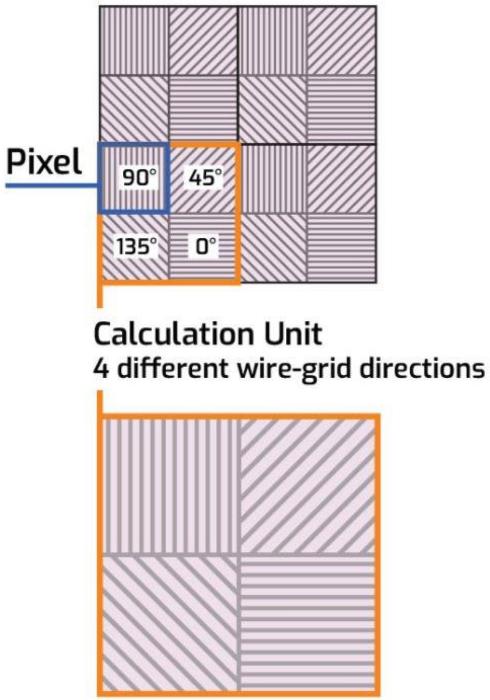

Two Depolarizing Samples

- Roughened LEGO bricks
  - Ensemble of samples with same material, different textures
  - Depolarization magnitude expected to trend with roughness

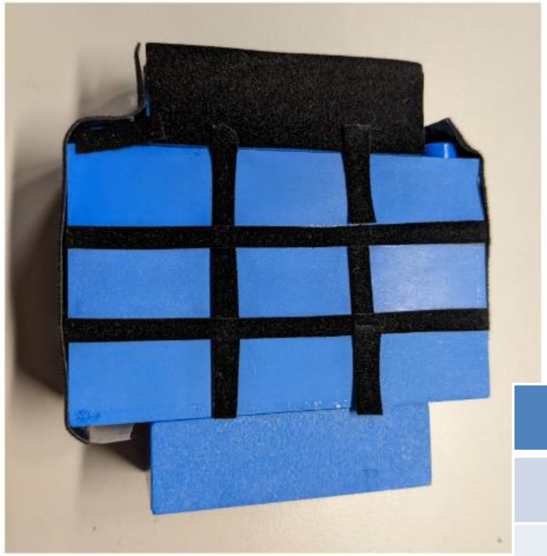

Roughness Averages [μm]		
0.49	0.56	3.35
3.55	2.62	0.35
1.68	1.26	6.32

- 3D printed sphere and Stanford bunny
  - Pair of samples with same material, different shapes
  - Same pBRDF should apply but different levels of complexity in geometry

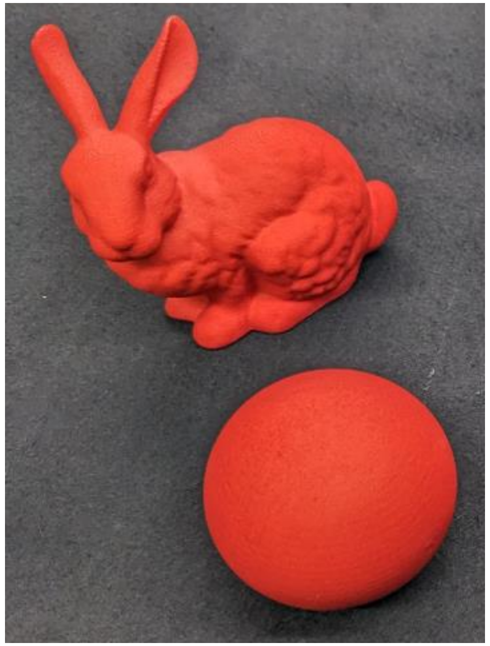

Roughened LEGOS with First-Surface Model

Mueller polarimeter
(40 measurements)

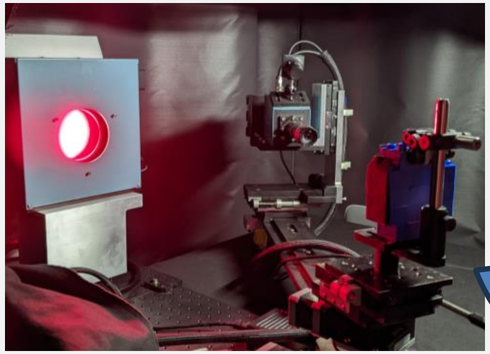

Roughness Averages [μm]		
0.49	0.56	3.35
3.55	2.62	0.35
1.68	1.26	6.32

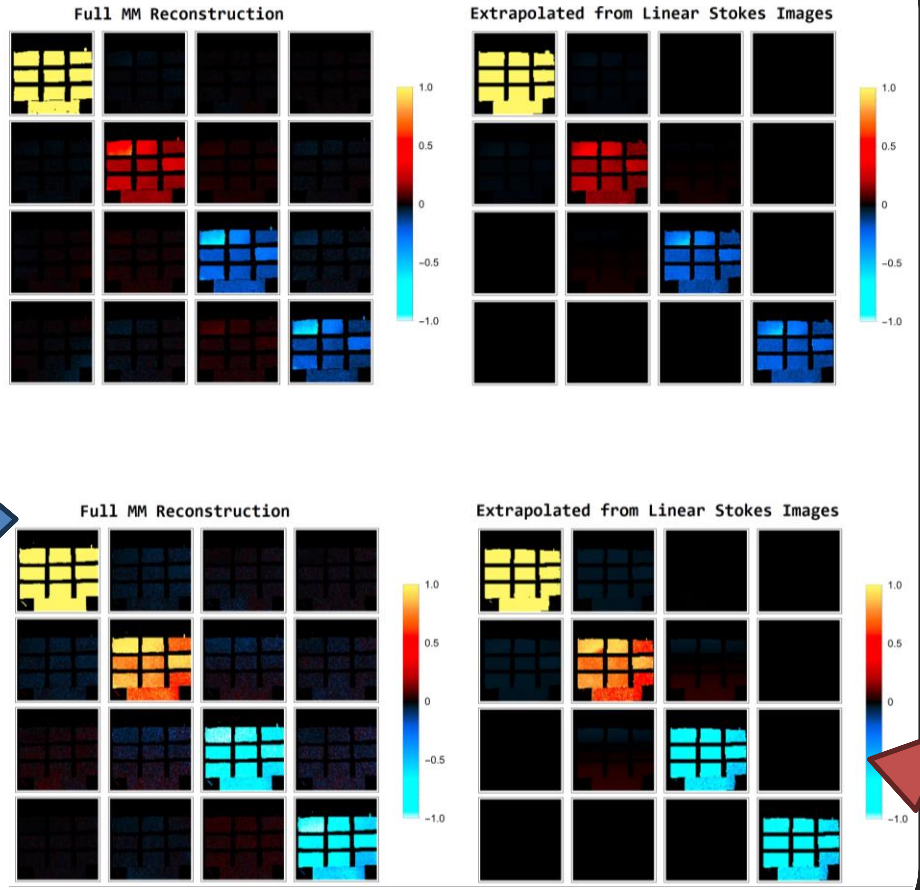

Partial polarimeter
(4 measurements)

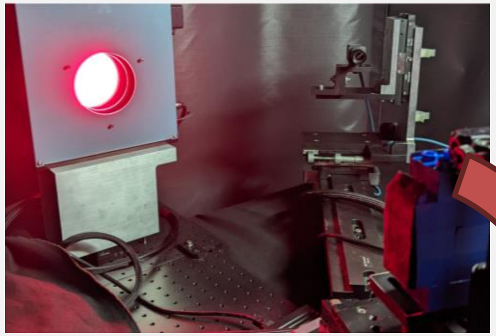

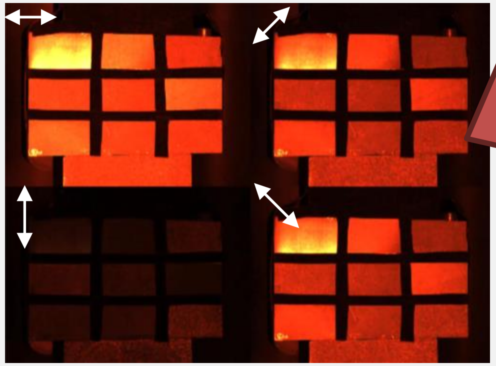

Partial polarimetric data

- MM image extrapolated from 10x fewer measurements
- Extrapolated MMs predict subsequent polarimetric measurements with average of 6% error

3D Printed Objects with Mixed Model

- Average ξ_0 error of 7.6% for spheres with 4 measurements versus 40 measurements

- Extrapolated MM images for bunnies used to predict polariscopic images

Depolarization parameter ξ_0 images

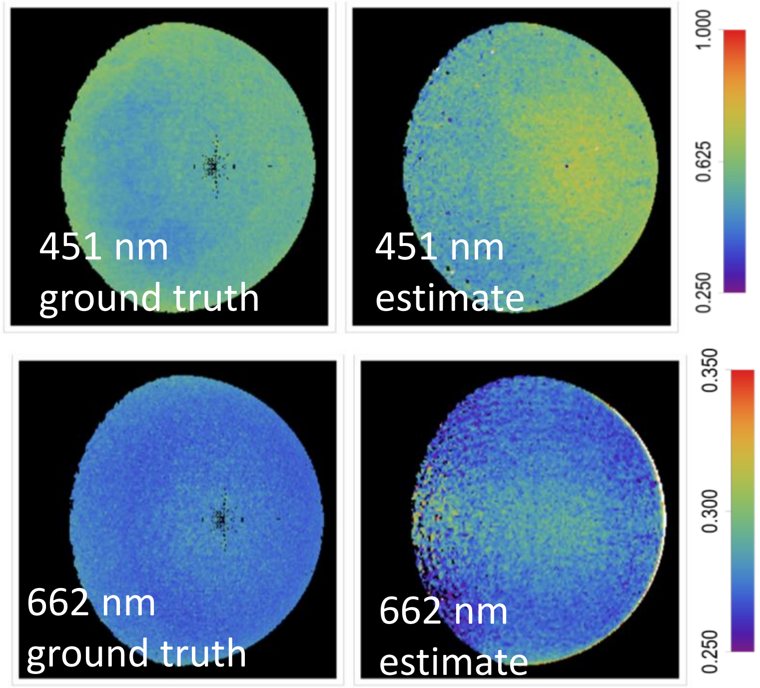

Pixelwise depolarization error

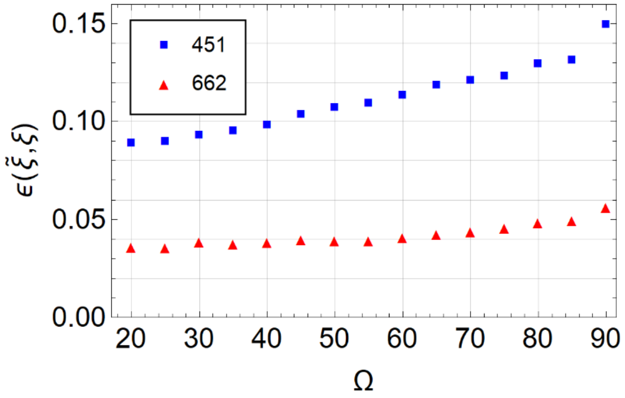

Predicted polariscopic images

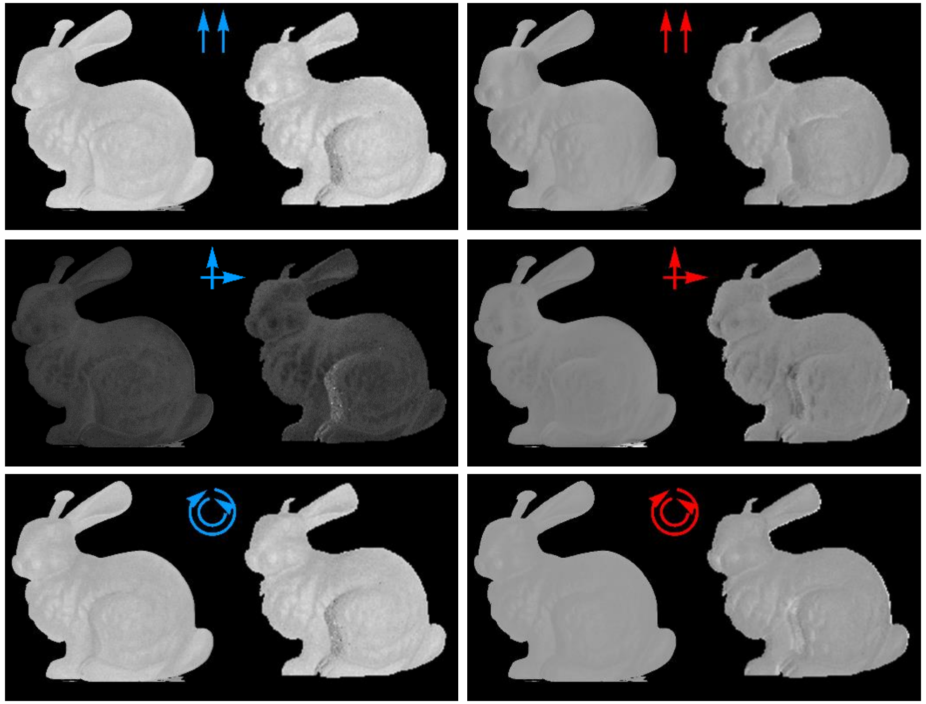

Summary and Conclusion

Chapter 7

Summary

- Contributions of this doctoral research are:

1. Optimization of polarization generator and analyzer states for maximizing contrast in polariscopic images of birefringent targets which is demonstrated on *in vivo* human eyes,

2. A method for efficiently acquiring and representing empirical MM data as a function of scattering geometry which requires 37% fewer goniometric measurements and stores 3 times fewer MMs per wavelength than the state-of-the-art,

3. An original polarized scattering model which both decouples depolarization and mixes first-surface with diffuse polarized reflection as a function of scattering geometry, with an average diattenuation orientation error of 10.9° and magnitude error of 8.3% when compared to measured data, and

4. A partial polarimetric method for estimating depolarization magnitude and extrapolating MM, which resulted in an average error in depolarization magnitude of 7.6% and simulated polarimetric measurement error of 6.0% despite a 10× reduction in number of measurements.

Conclusion

- As polarimetric sensing technologies become more mature and widely accessible, there will be an abundance of new potential applications for polarization imaging
- Full MM polarimetry may be required to realize some applications, others may only require partial polarimetric information
- Assessment of which partial polarimetric technologies and strategies are most useful for particular applications depend on understanding of the polarization phenomena
- Contributions of this dissertation represent different efforts to reduce some complexities of polarimetric imaging
  - Through these simplifications, insights from polarimetric information may be more easily accessed in variety of applications

Thanks!!

Analyzing Mueller Image Data

Levels of Approximation

1. Full Mueller matrix

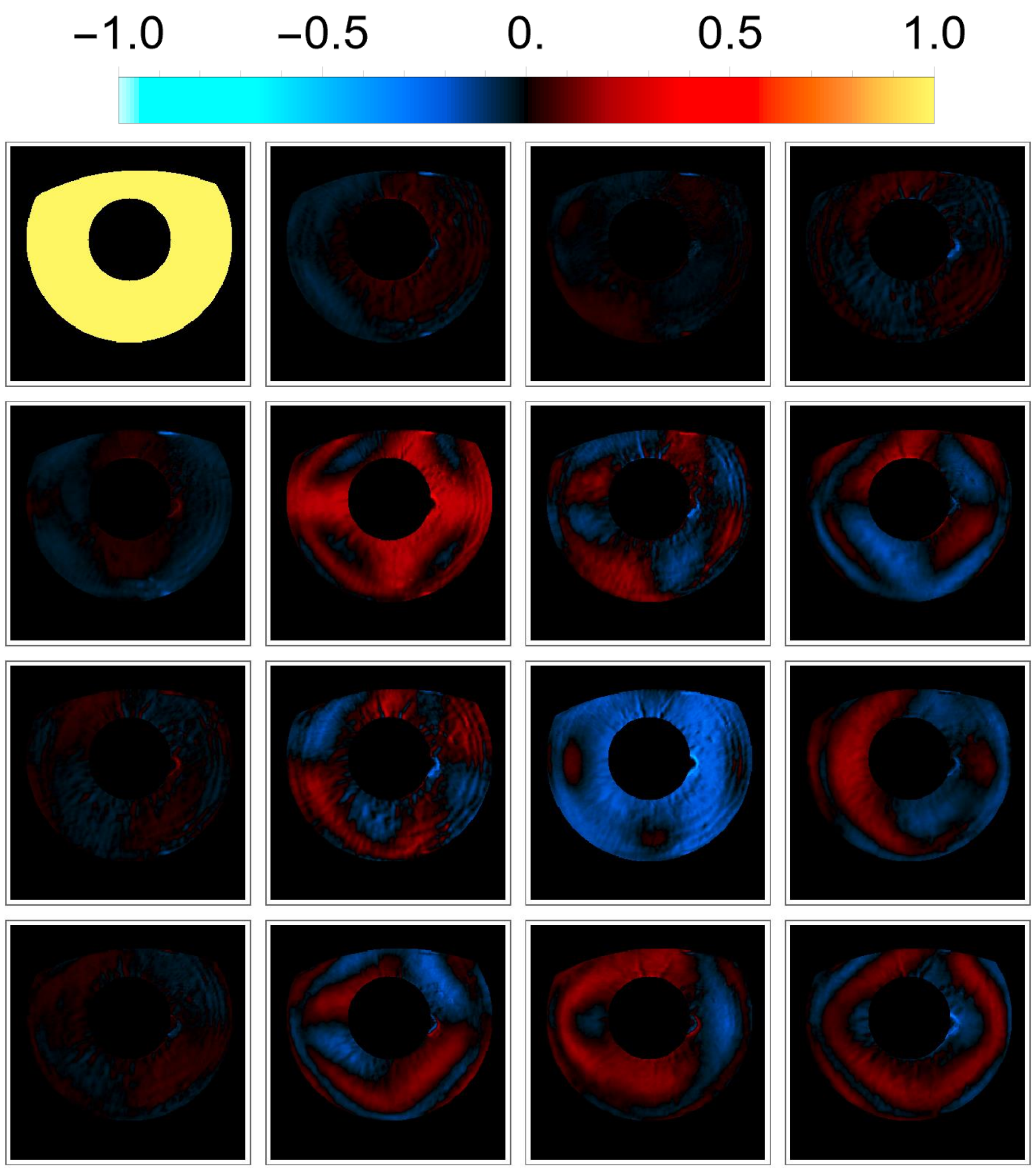

Assumptions of Uniform Properties

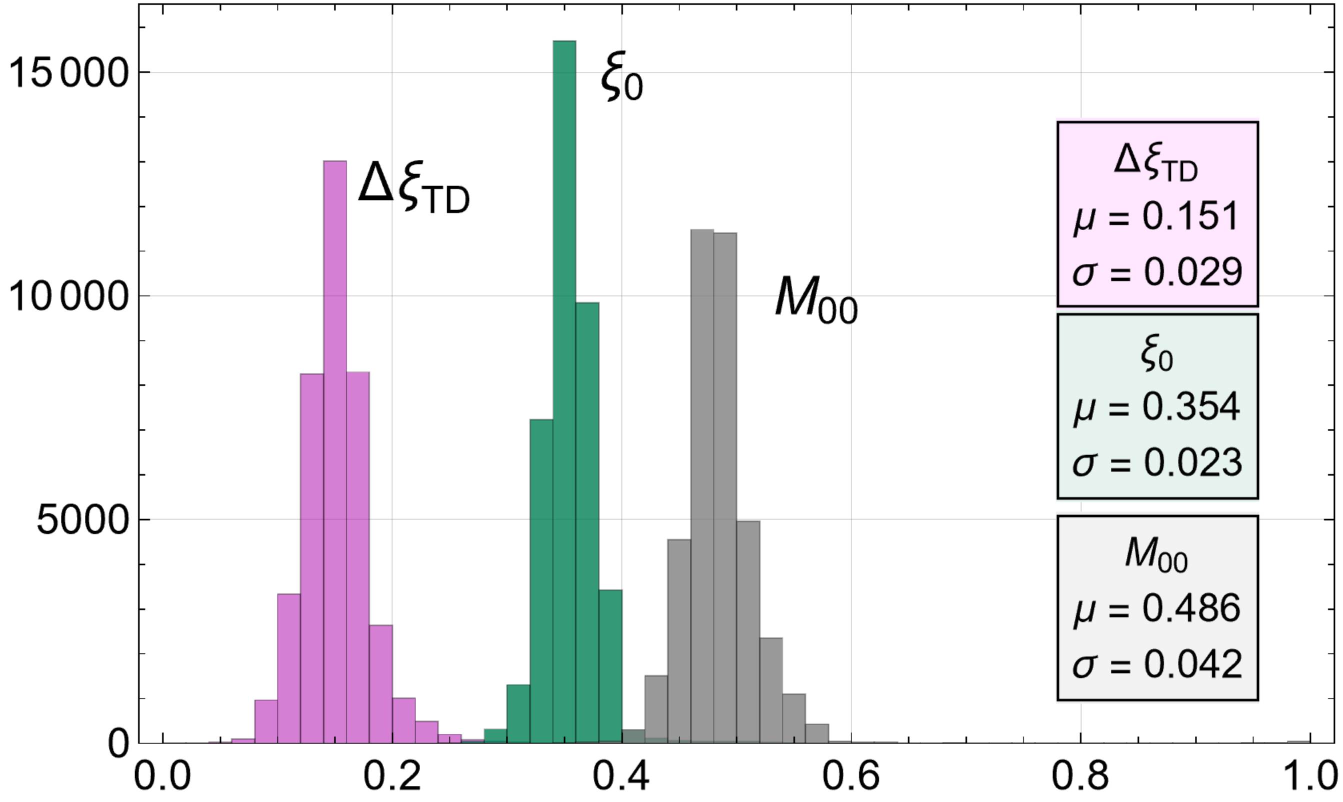

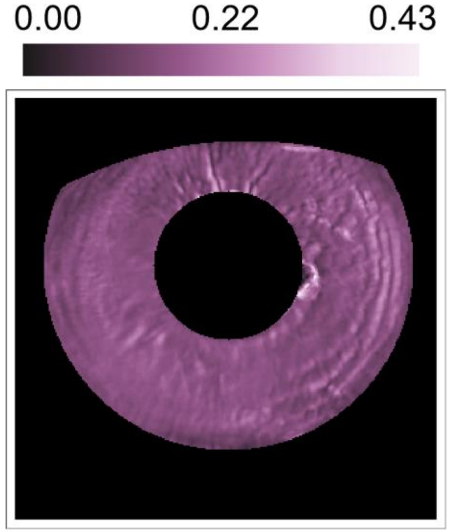

$\Delta\xi_{TD}$ Image

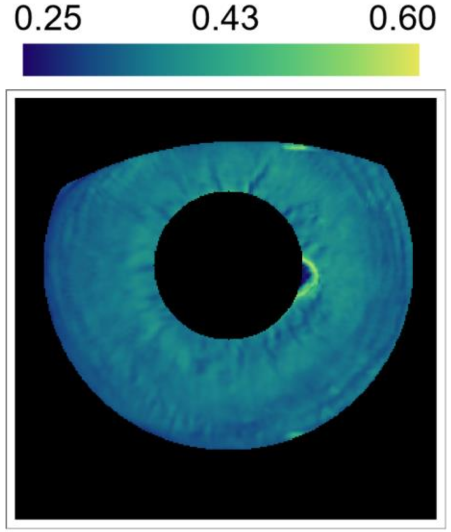

ξ_0 Image

- $\Delta\xi_{TD}$ - indicates appropriateness of 1st order depolarization approximation
- ξ_0 - depolarization magnitude parameter
- M_{00} - average reflectance

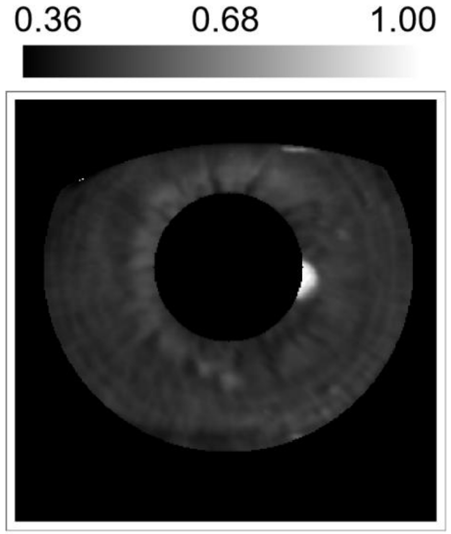

M_{00} Image

Elliptical Retardance of Cornea

Retardance Vector

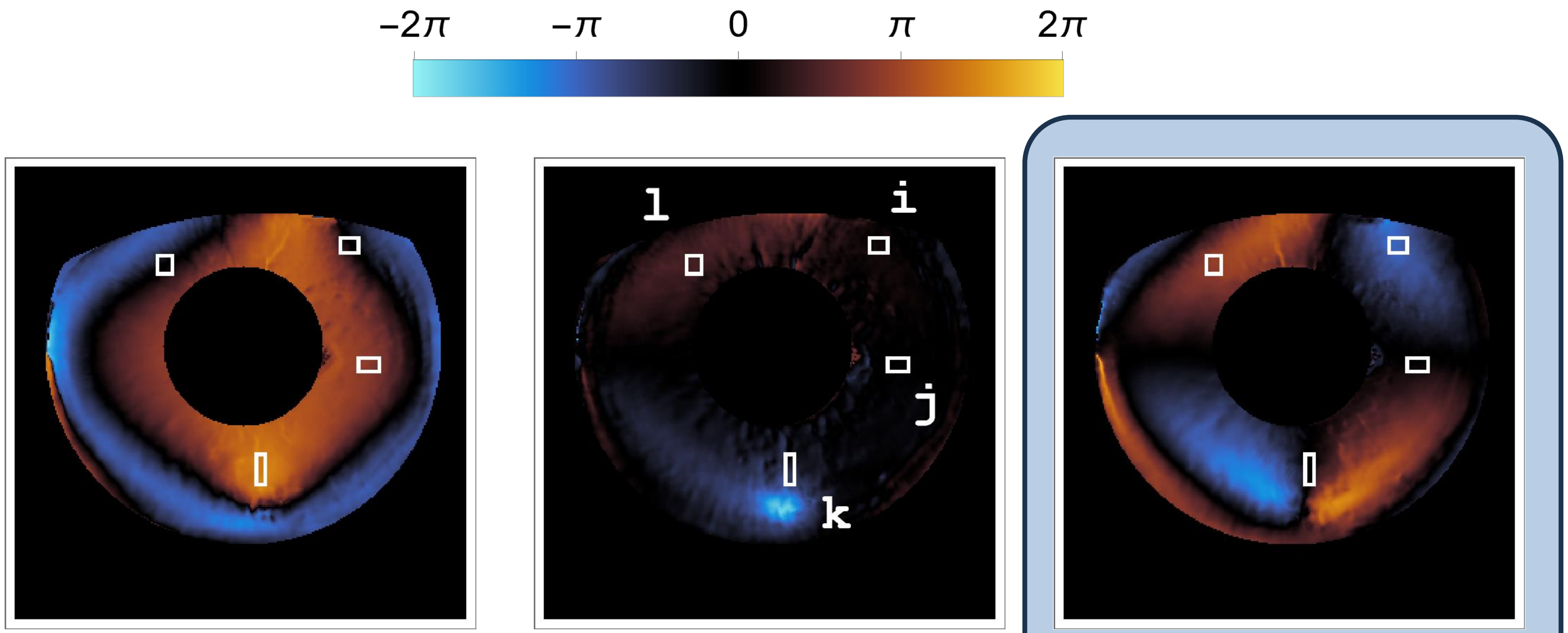

δ_H δ_{45} δ_R

Retarder Space

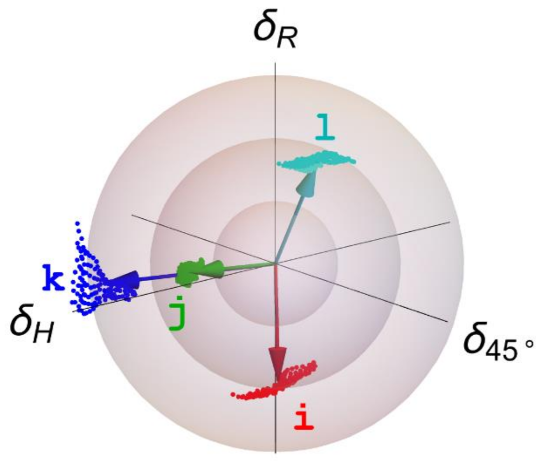

$\vec{\boldsymbol{\delta}}$

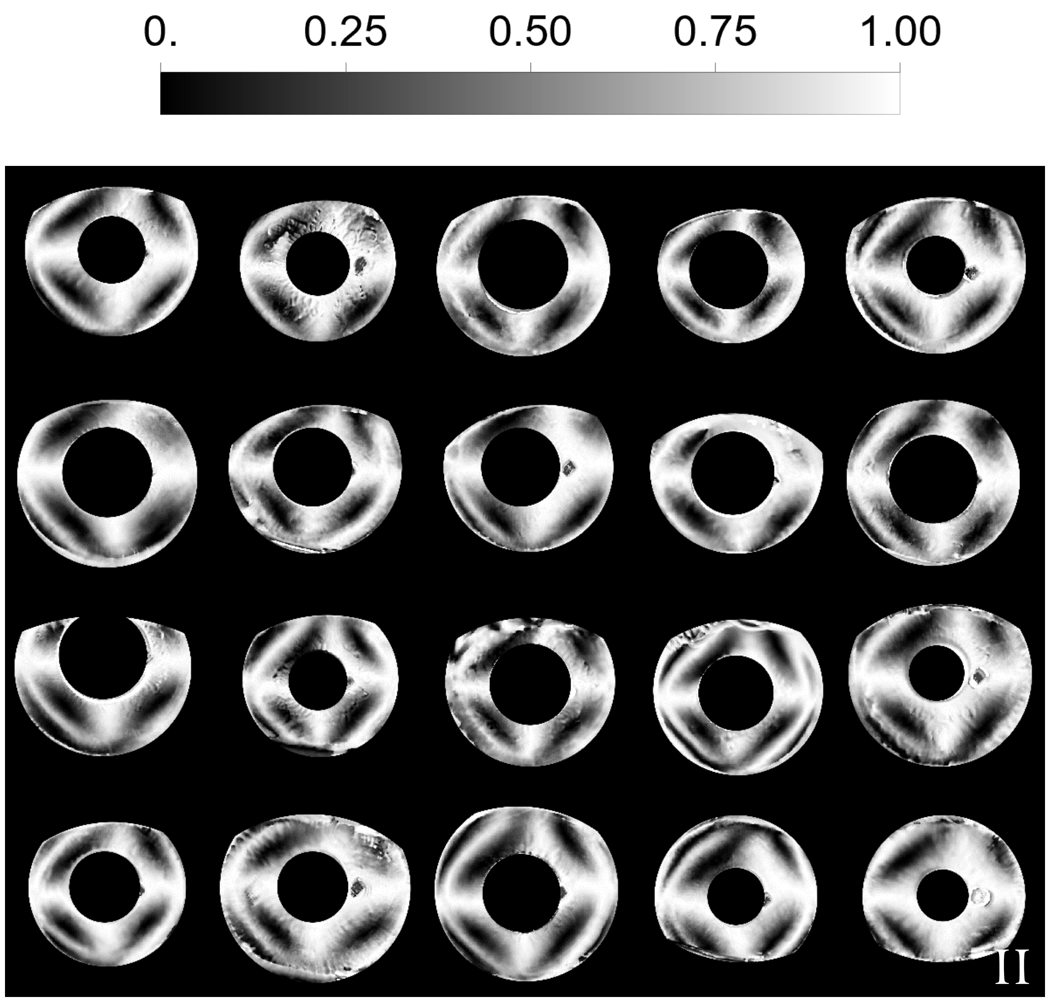

Expected patterns for 20 individuals

Eye Database

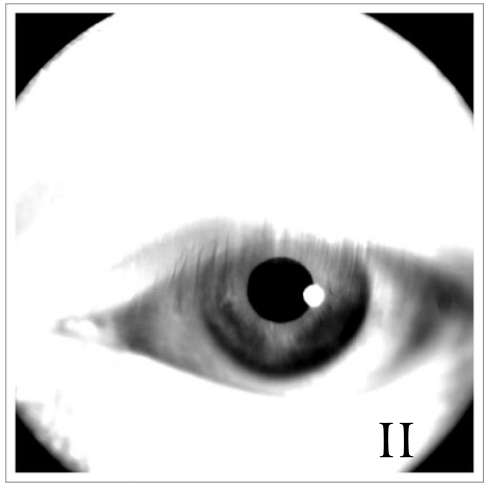

- Special thanks to Adeline Tai for performing the MM measurements
- Dataset of eye MM images is publicly available: https://doi.org/10.25422/azu.data.24722358

Collagen Fibrils

- Stroma layer of cornea consists of collagen fibrils
- Fibrils give cornea anisotropic structure which produces birefringence
- Cascade of linear retarders with varying fast axes can produce elliptical retardance
  - One potential explanation for observed circular retardance

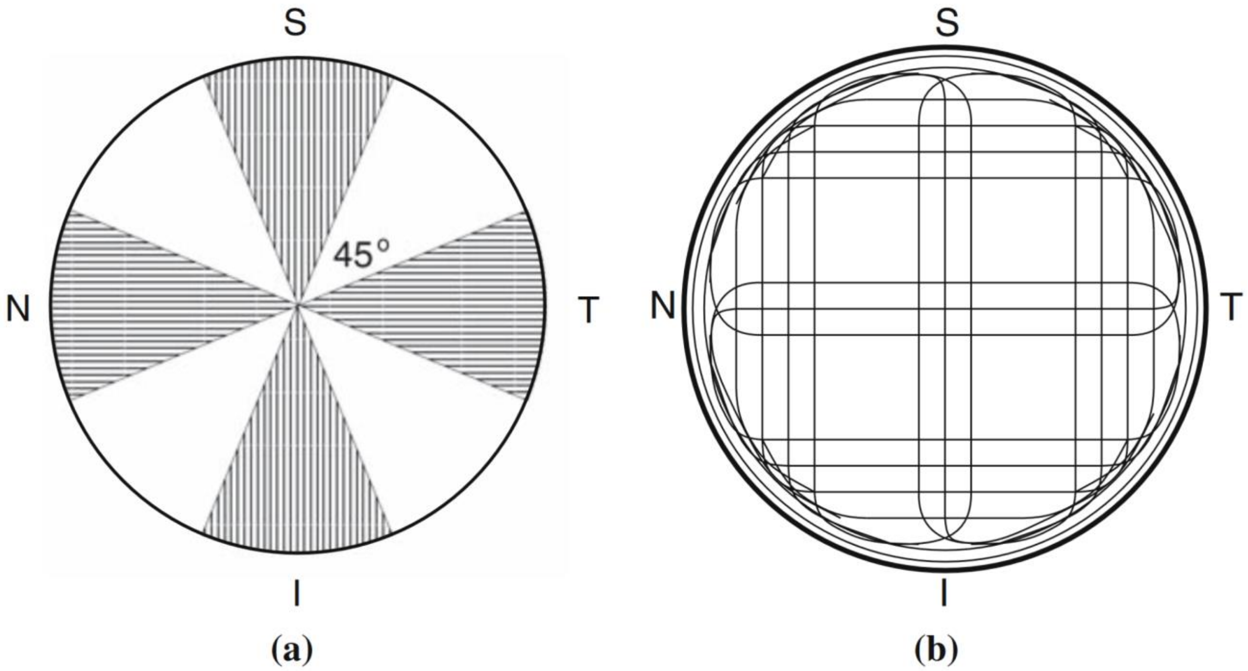

Newton, & Meek, K. M. (1998). The Integration of the Corneal and Limbal Fibrils in the Human Eye. *Biophysical Journal*, *75*(5), 2508–2512. https://doi.org/10.1016/S0006-3495(98)77695-7

Rusinkiewicz Angles

- Images of Rusinkiewicz angles captured for different shapes
- Sphere captures most unique geometries, plane captures least
- Precompute captured Rusinkiewicz angles for a particular goniometer sequence, compare sequences

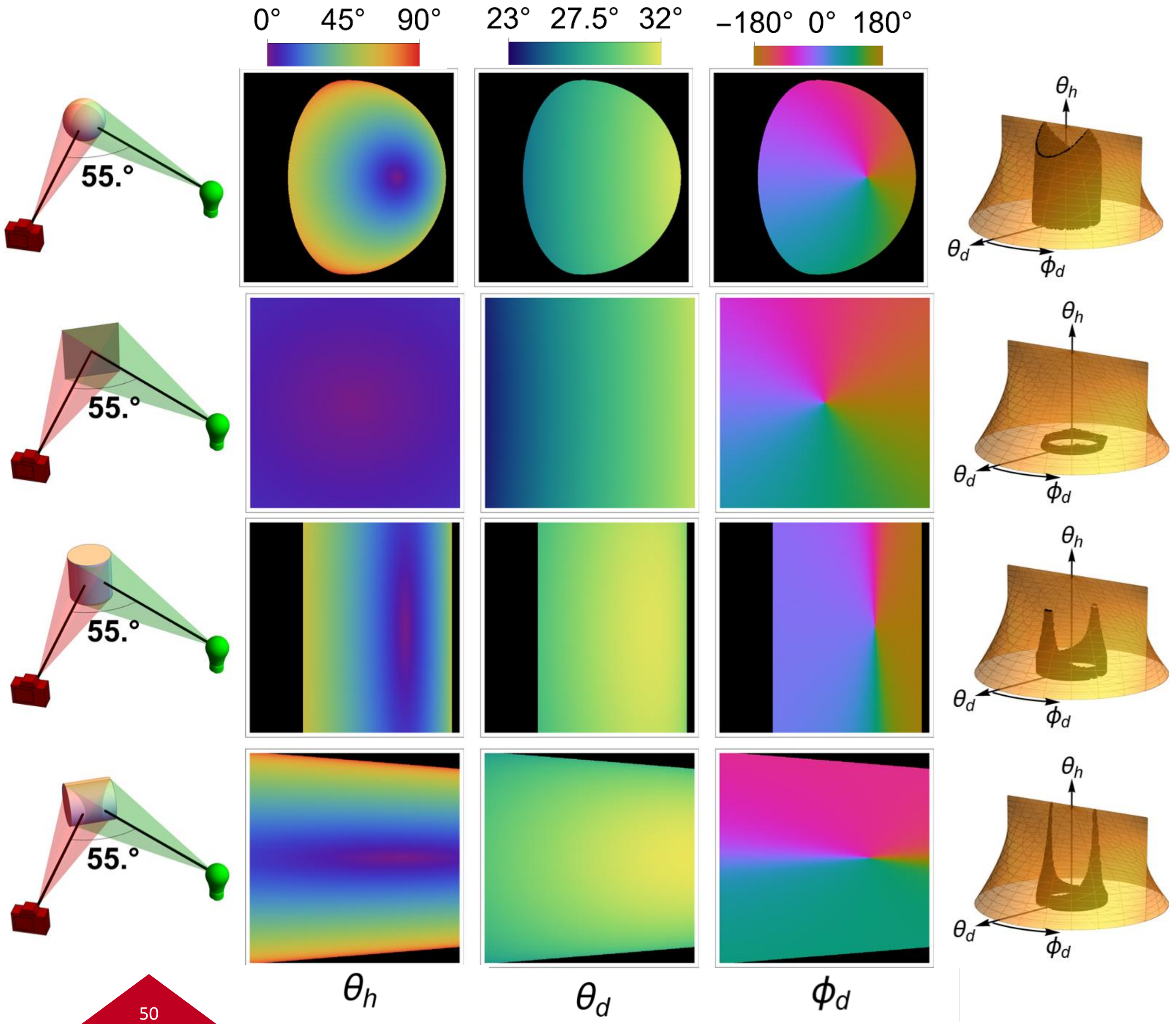

Tabulated pBRDF File Comparison

- KAIST:
  - 147 goniometer positions per wavelength
  - 912 MB for 5 wavelengths
  - 2,989,441 MMs per wavelength
  - Saved as multidimensional table where table index corresponds to $(\theta_h, \theta_d, \phi_d, \lambda)$
  - Includes non-reflection geometries
  - Includes redundant geometries
  - Can be used directly in rendering engine

- UA:
  - 92 goniometer positions per wavelength
  - 331 MB for 5 wavelengths (we will only have 3)
  - 1,086,904 MMs per wavelength
  - Saved as single list of MMs, related to Rusinkiewicz angles by angle key
  - Includes only reflection geometries
  - Includes only unique geometries
  - Cannot be used directly in rendering engine (yet)

Baek, Seung-Hwan, et al. "Image-Based Acquisition and Modeling of Polarimetric Reflectance." ACM Transactions on Graphics, vol. 39, no. 4, 12 Aug. 2020

Triple-degenerate MM Model

- Useful special case of Cloude spectral decomposition has “triple-degenerate“ (TD) eigenspectrum

- Convex sum of non-depolarizing matrix and ideal depolarizer matrix

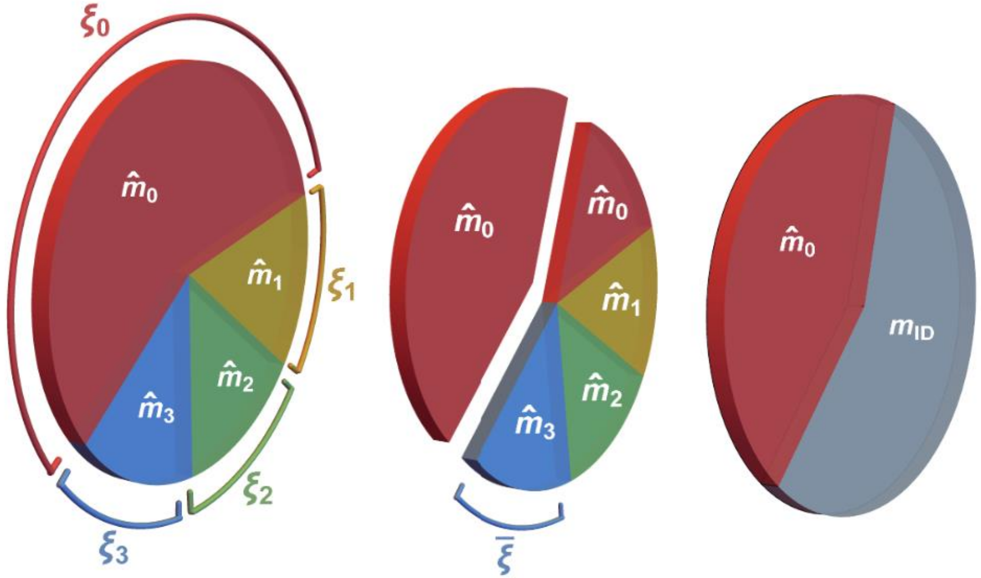

(a) Cloude decomposition (b) Equal Weights (c) TD Model

$$\mathbf{M} = \sum_{n=0}^{3} \xi_n \widehat{\mathbf{M}}_n,$$

$$\mathbf{M} = \frac{4M_{00}}{3}\left[\left(\xi_0 - \frac{1}{4}\right)\widehat{\mathbf{M}}_0 + (1-\xi_0)\,\mathbf{M}_{ID}\right]$$

Mixed Polarization Model

- pBRDF can be applied to more complex geometries
- Shadow and masking (adjacency effects) of microfacet distribution are absorbed into other model terms
- Model only describes polarimetry, not radiometry (MM is normalized)

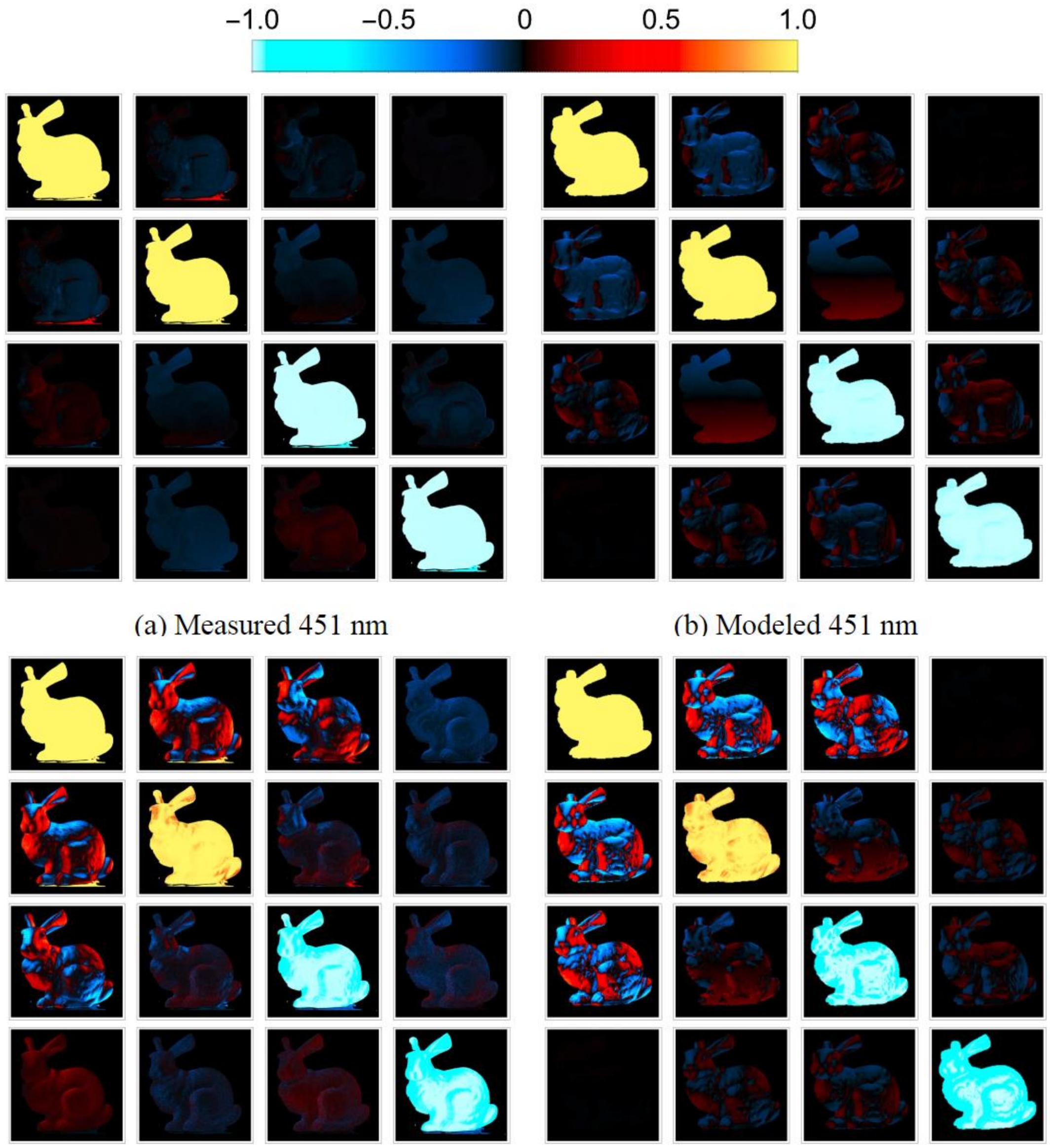

(a) Measured 451 nm (b) Modeled 451 nm

(c) Measured 662 nm (d) Modeled 662 nm

Diattenuation Comparison

- Diattenuation orientation images show match in spatial trend

- Pixel-wise errors low for 451 nm which has less spatial variation, higher errors for 662 nm

- Over wavelength and geometry, average diattenuation orientation error of 10.9° and magnitude error of 8.3%

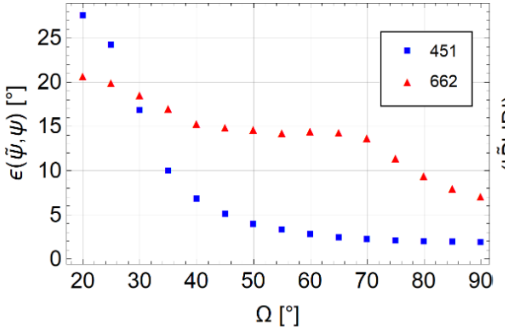

(a) Diattenuation orientation error

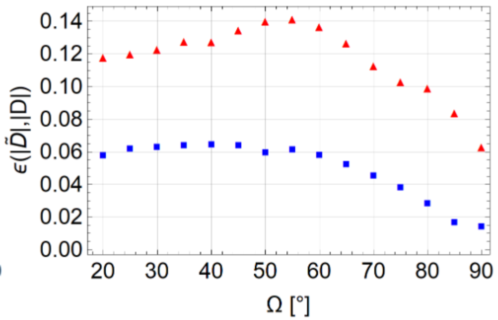

(b) Diattenuation magnitude error

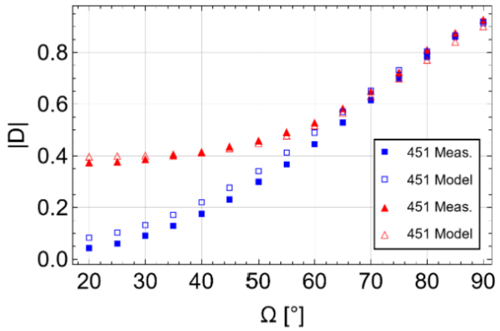

(c) Average diattenuation magnitude

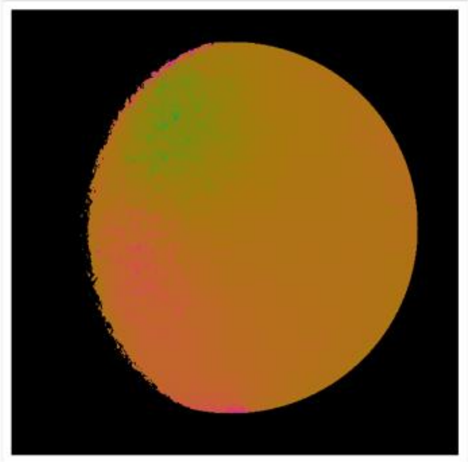

(a) Measured ψ 451 nm

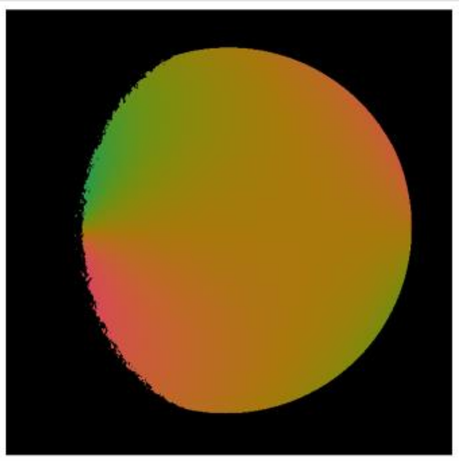

(b) Modeled $\tilde{\psi}$ 451 nm

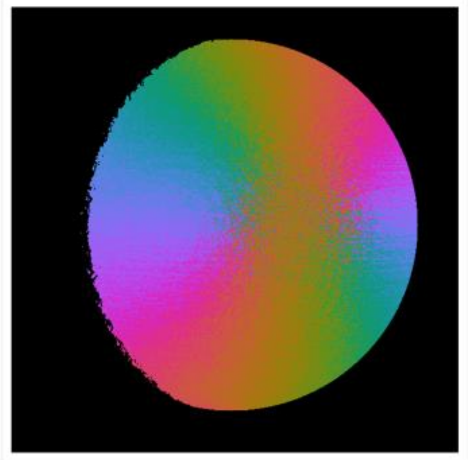

(d) Measured ψ 662 nm

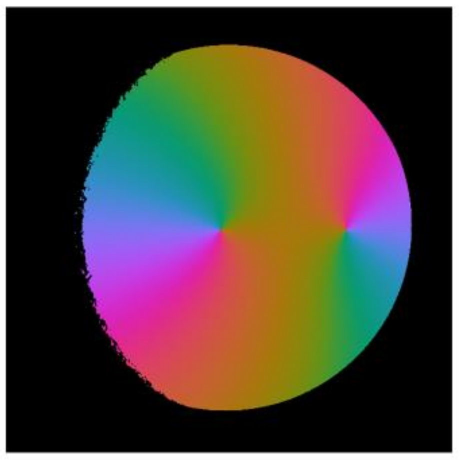

(e) Modeled $\tilde{\psi}$ 662 nm

3D Printed Objects with Mixed Model

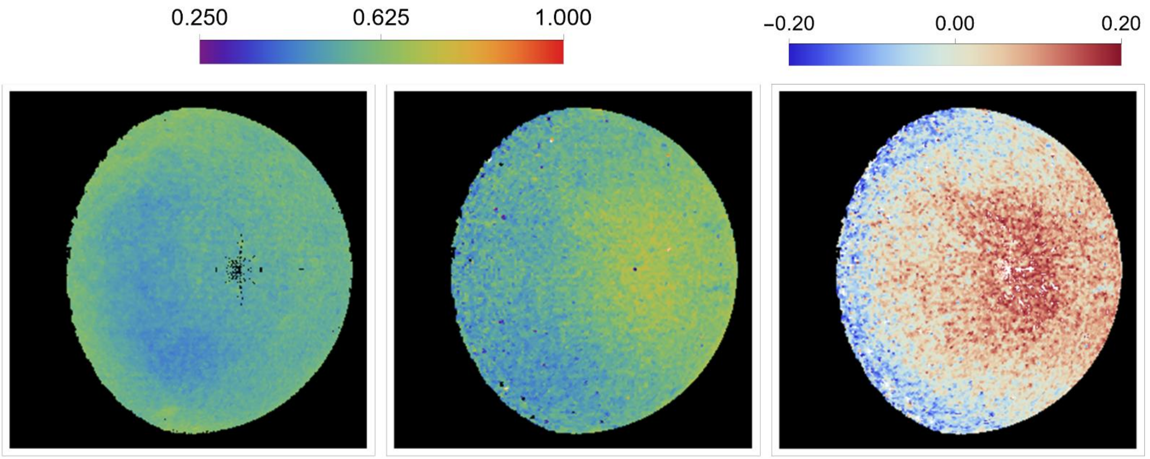

(a) True ξ_0 451 nm (b) Estimated $\tilde{\xi}_0$ 451 nm (c) ξ_0 deviation 451 nm

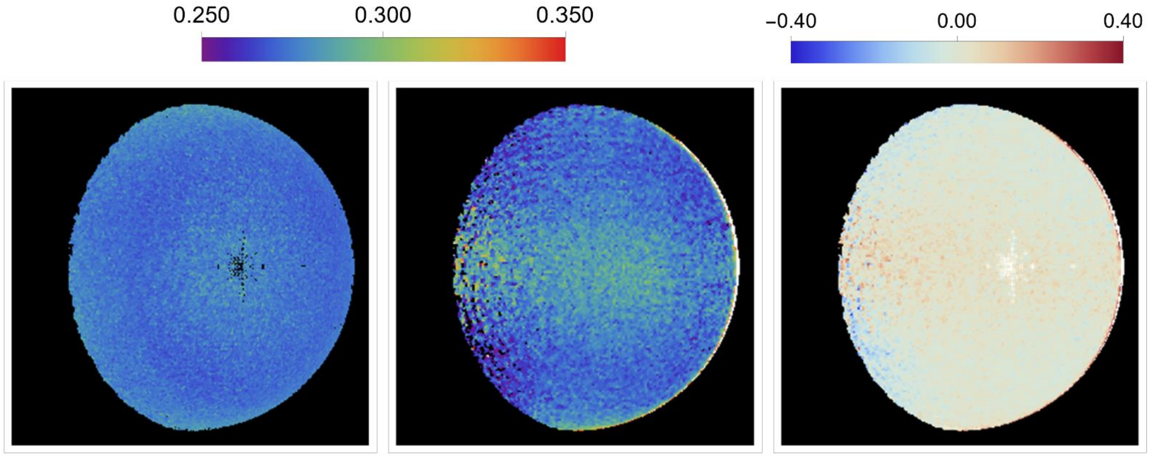

(d) True ξ_0 662 nm (e) Estimated $\tilde{\xi}_0$ 662 nm (f) ξ_0 deviation 662 nm

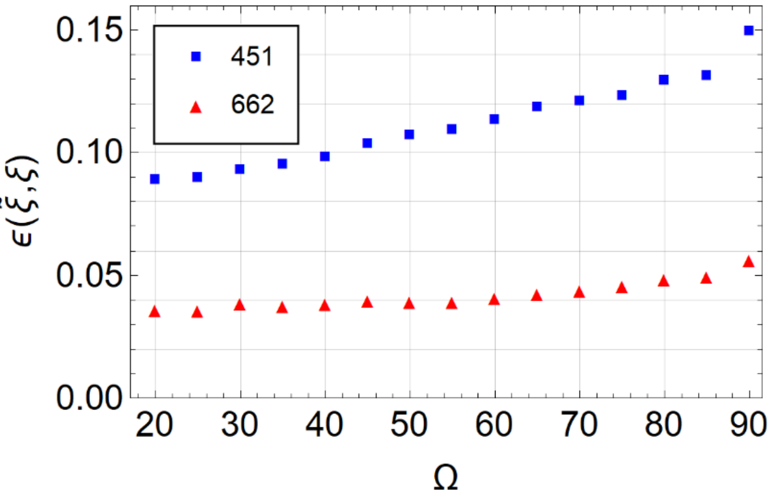

Average ξ_0 error of 7.6%

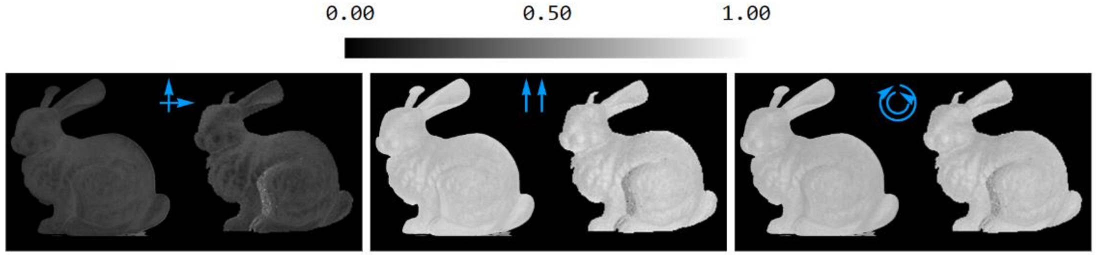

(a) Crossed linear polarizers 451 nm (b) Aligned linear polarizers 451 nm (c) Crossed circular polarizers 451 nm

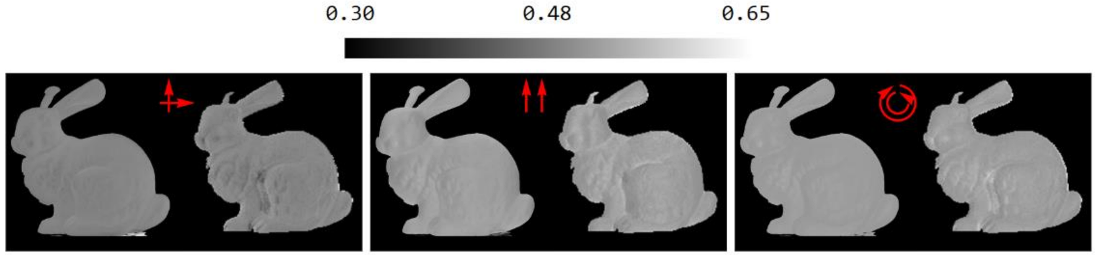

(d) Crossed linear polarizers 662 nm (e) Aligned linear polarizers 662 nm (f) Crossed circular polarizers 662 nm